Bioorganic Chemistry 117 (2021) 105425

Contents lists available at ScienceDirect

Bioorganic Chemistry

journal homepage: www.elsevier.com/locate/bioorg

Continuous Sirtuin/HDAC (histone deacetylase) activity assay using thioamides as PET (Photoinduced Electron Transfer)–based fluorescence quencher

Matthes Zessin [a], Marat Meleshin [b], Zeljko Simic [b], Diana Kalbas [b], Miriam Arbach [b], Philip Gebhardt [b], Jelena Melesina [a], Sandra Liebscher [c], Frank Bordusa [c], Wolfgang Sippl [a], Cyril Barinka [d], Mike Schutkowski [b,*]

[a] Department of Medicinal Chemistry, Institute of Pharmacy, Martin Luther University Halle-Wittenberg, Halle/Saale, Germany
[b] Department of Enzymology, Charles Tanford Protein Center, Institute of Biochemistry and Biotechnology, Martin Luther University Halle-Wittenberg, Halle/Saale, Germany
[c] Department of Natural Product Biochemistry, Charles Tanford Protein Center, Institute of Biochemistry and Biotechnology, Martin Luther University Halle-Wittenberg, Halle/Saale, Germany
[d] Institute of Biotechnology of the Czech Academy of Sciences, BIOCEV, Prumyslova 595, 252 50 Vestec, Czech Republic

ARTICLE INFO

Keywords:
Sirtuin assay
HDAC11 assay
Thioamide
Photoinduced electron transfer quenching
Microtiter plate-based screening
Histone deacetylase (HDAC) inhibitor

ABSTRACT

Histone deacylase 11 and human sirtuins are able to remove fatty acid-derived acyl moieties from the ε-amino group of lysine residues. Specific substrates are needed for investigating the biological functions of these enzymes. Additionally, appropriate screening systems are required for identification of modulators of enzymatic activities of HDAC11 and sirtuins. We designed and synthesized a set of activity probes by incorporation of a thioamide quencher unit into the fatty acid-derived acyl chain and a fluorophore in the peptide sequence. Systematic variation of both fluorophore and quencher position resulted "super-substrates" with catalytic constants of up to 15,000,000 $M^{-1}s^{-1}$ for human sirtuin 2 (Sirt2) enabling measurements using enzyme concentrations down to 100 pM in microtiter plate-based screening formats. It could be demonstrated that the stalled intermediate formed by the reaction of Sirt2-bound thiomyristoylated peptide and NAD^+ has IC_{50} values below 200 pM.

1. Introduction

Acylation of lysine side chains in proteins is a widespread post-translational modification regulated by the action of acyltransferases or by the existing metabolic situation. Reversal of such lysine acylations is mediated by evolutionary conserved enzymes known as histone deacetylases (HDACs). Based on sequence homology, HDACs can be divided into 4 classes. Members of class I (HDAC 1, 2, 3, and 8), class IIa (HDAC4, 5, 7 and 9), class IIb (HDAC6 and 10), and class IV (HDAC11) are Zn^{2+} dependent hydrolases, while class III proteins (called sirtuins; Sirt1 – 7) use NAD^+ as a co-substrate. They transfer the acyl moiety to the ADP-ribosyl fragment of the co-substrate thereby generating 2-O-acetyl-ADP-ribose and nicotinamide as the third reaction product [1].

Enzymatic activity of HDACs is involved in various (patho)physiological processes including cancer progression, regulation of obesity and immune function. Therefore, several HDAC inhibitors have been approved by the Food and Drug Administration for the treatment of cancer (vorinostat, romidepsin, belinostat, and panobinostat) and a number of clinical trials with sirtuin inhibitors (either natural products or synthetic small molecules) have been started to evaluate their efficacy. Robust and continuous sirtuin/HDAC activity assays compatible with high-throughput screening (HTS) are still required for further drug development.

Several assays have been developed for the monitoring of sirtuin and HDAC activity as reviewed in references [2–3]. Most of these activity assays are discontinuous (HPLC-based or mass spectrometry-based

Abbreviations: TFA, trifluoroacetic acid; Mcm, 7-methoxy-coumaryl-L-alanine; Abz, 2-aminobenzoyl; Ac, acetyl; HTS, high-throughput screening. HDAC, histone deacetylase; Sirt, sirtuin; PET, photoinduced electron transfer.

* Corresponding author.
E-mail address: mike.schutkowski@biochemtech.uni-halle.de (M. Schutkowski).

https://doi.org/10.1016/j.bioorg.2021.105425
Received 20 July 2021; Received in revised form 7 October 2021; Accepted 9 October 2021
Available online 12 October 2021

assays) or suffering from complex reaction mixtures caused by coupled enzymatic or chemical reactions requiring additional control measurements. Determination of IC_{50} or K_i-values for inhibitors is therefore time-consuming and cumbersome. Nearly all sirtuins have demyristoylation activity [4] and recently it was shown that HDAC11 is a robust demyristoylase as well [5–7]. We were able to demonstrate that the replacement of a myristoylated lysine residue (Fig. 1B) in TNFα-derived substrate peptides by an N-(2-aminobenzoyl)-11-aminoundecanoylated lysine residue (Fig. 1C) generates a quasi-universal sirtuin substrate enabling continuous activity measurements by fluorescence [8]. Recently, we demonstrated that the same peptide derivative is suitable for recording of enzymatic activity of HDAC11, enabling re-evaluation of HDAC11 inhibitors [9]. Nevertheless, attempts to increase the size of the fluorophore in the acyl moiety of the acylated lysine residue of such substrates, in order to allow fluorescence measurements at longer wavelengths, lead to dramatically decreased catalytic efficiency for sirtuins [8] and HDAC11 [9]. Additionally, Kawaguchi *et al.* were able to show that Sirt1-3 and Sirt6 are able to recognize a DABCYL moiety in the acyl chain (Fig. 1D) enabling monitoring of sirtuin activity in living cells [10]. Recently, the DABCYL quencher was replaced by Disperse Red derivative (Fig. 1E) yielding fluorescence probes with improved substrate properties for sirtuin activity measurements [11]. In our search for small quenchers of fluorescence we found thioamides to be ideal candidates. Caused by the soft sulfur atom in the thioamide moiety fluorescence quenching is possible via a mechanism called photoinduced electron transfer (PET) [12]. The Petersson group used this quenching principle for monitoring of protein folding [12–15], recording of proteolytic activities [15–17], investigation of binding events [18] and recently for the analysis of mobility of polyproline ruler peptides [19]. Additionally, we demonstrated that replacement of the scissile bond in fluorescently labeled HDAC substrates by a thioamide bond enabled continuous activity determination of HDAC8 and HDAC11 (Fig. 1F) via

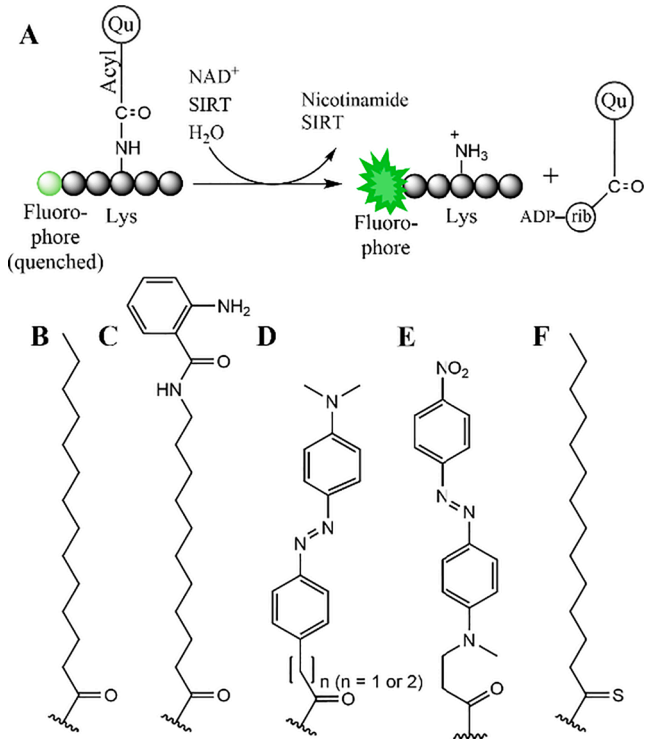

Fig. 1. Scheme of the sirtuin-mediated deacylation reaction. A shows a quencher (Qu)-containing acyl residue being transferred from the lysine side chain to ADP-ribose (ADP-rib) resulting in an increasing fluorescence intensity of the fluorophore incorporated in the peptide backbone. **B.** shows the naturally occurring myristoyl residue. **C-G** shows different acyl residues derived of the myristoyl residue used for HDAC/sirtuin activity assays.

PET fluorescence quenching [3]. Unfortunately, amide to thioamide replacement to the scissile bond leads to very poor substrates for sirtuins because of the generation of a so-called stalled intermediate, slowing down the reaction rate dramatically [20], and thiomyristoyl residue (Fig. 1F) represents a key structural element of efficient inhibitors for Sirt1-3 and Sirt6 [21–23]. To circumvent this problem, we introduced a thioamide bond into the myristoylated lysine residue (Fig. 2, R4) and were able to show that such substrates are well recognized by sirtuins and HDAC11 following the assay principle shown in Fig. 1A. Moreover, incorporation of different fluorophores (Fig. 2) into the peptide chain in combination with thioacetylated 11-aminoundecanoyl lysine residues (Fig. 2, R4) yielded sirtuin and HDAC11 substrates with superior catalytic constants in a continuous and direct activity assay. Such "super-substrates" with catalytic constants of up to 15,000,000 $M^{-1}s^{-1}$ for Sirt2 are useful for microtiter plate-based screening in 1,536-well format with Z'-factors higher than 0.88.

2. Results

All the compounds were synthesized based on a short TNFα-derived peptides because this sequence was used as a model substrate [21,24–25] for different sirtuin isoforms (Fig. 2, 1a). Fmoc-based solid phase peptide chemistry was used in combination with the nosyl-protecting group enabling selective on-resin modification of the respective lysine side chain. All compounds have purity greater than 95% as determined by HPLC at 220 nm and showed the expected molecular mass (Figures S1-S26 and Table S1). Peptide **1a** (Fig. 2) was reported to be a substrate for Sirt2 and Sirt3 with specificity constants of 53,000 $M^{-1}s^{-1}$ and 29,500 $M^{-1}s^{-1}$ [8], respectively, and represents the best Sirt6 substrate described so far [24]. The peptide derivatives were synthesized with selectively modified myristoyl residues. In a systematic work, we replaced two adjacent methylene groups by a thioamide group ranging from methylenes 3/4 to 13/14 (a thioamide scan) resulting in 11 peptides with the thioamide moiety in different positions (Table S2). Analyzing substrate properties of these derivatives with Sirt2, Sirt3, Sirt5 and Sirt6 we found that thioamide substitutions in the distal end of the acyl chain are well tolerated (Fig. S27) with an optimum spanning methylenes 11/12, 12/13 and 13/14. Because it was known that acylated 11-aminoundecanoylated lysine residues are well accepted by sirtuins [8] we focused on thioacetylated 11-aminoundecanoyl moieties in this work (R4, Fig. 2). To assess whether a bulky fluorescein residue attached to a cysteine side chain is accepted by sirtuins we generated a control peptide **4b** (Fig. 2, R2). To our surprise the modified cysteine at the −2 position was well tolerated by both sirtuins and HDAC11 (Table 2). Additionally, we generated a control peptide **1b** with a non-modified amino acid sequence but replacement of the myristoyl residue by the thioacetylated 11-aminoundecanoyl moiety (R4, Fig. 2) to analyze the effect of substitution of two adjacent methylene moieties by a thioamide group on HDAC activity. Again, we found no negative effect on substrate properties for sirtuins and HDAC11 (Table 2). Next, we systematically analyzed efficacy of fluorescein quenching by the thioamide moiety (Table 1) by moving the fluorescein-modified cysteine residue from −5 to +2 position (relative to the acylated lysine) of the substrate resulting in peptide derivatives **1**–**7** (Fig. 2). The quenching efficacy of these derivatives ranged from 35% for **2** to 48% for **6** (Table 1). As a control, we replaced the thioamide in the peptide **4** by an amide bond yielding **4c**, thus abolishing fluorescence quenching as expected (Table 1). Moreover, we also investigated the quenching efficacy for different fluorophores in the +2 position because a bulky residue like fluorescein was well accepted. Therefore, we synthesized derivatives **8**–**11** and determined the differences in fluorescence as compared to the fully converted assay solution. We found weak quenching for the 7-nitrobenzoxadiazole fluorophore (**11**) and for the BODIPY 507/545 dye (**8**). Surprisingly, fluorescence of structurally related BODIPY FL dye in **9** was quenched by more than 50% by the thioamide moiety.

To improve the quenching, we simultaneously substituted two

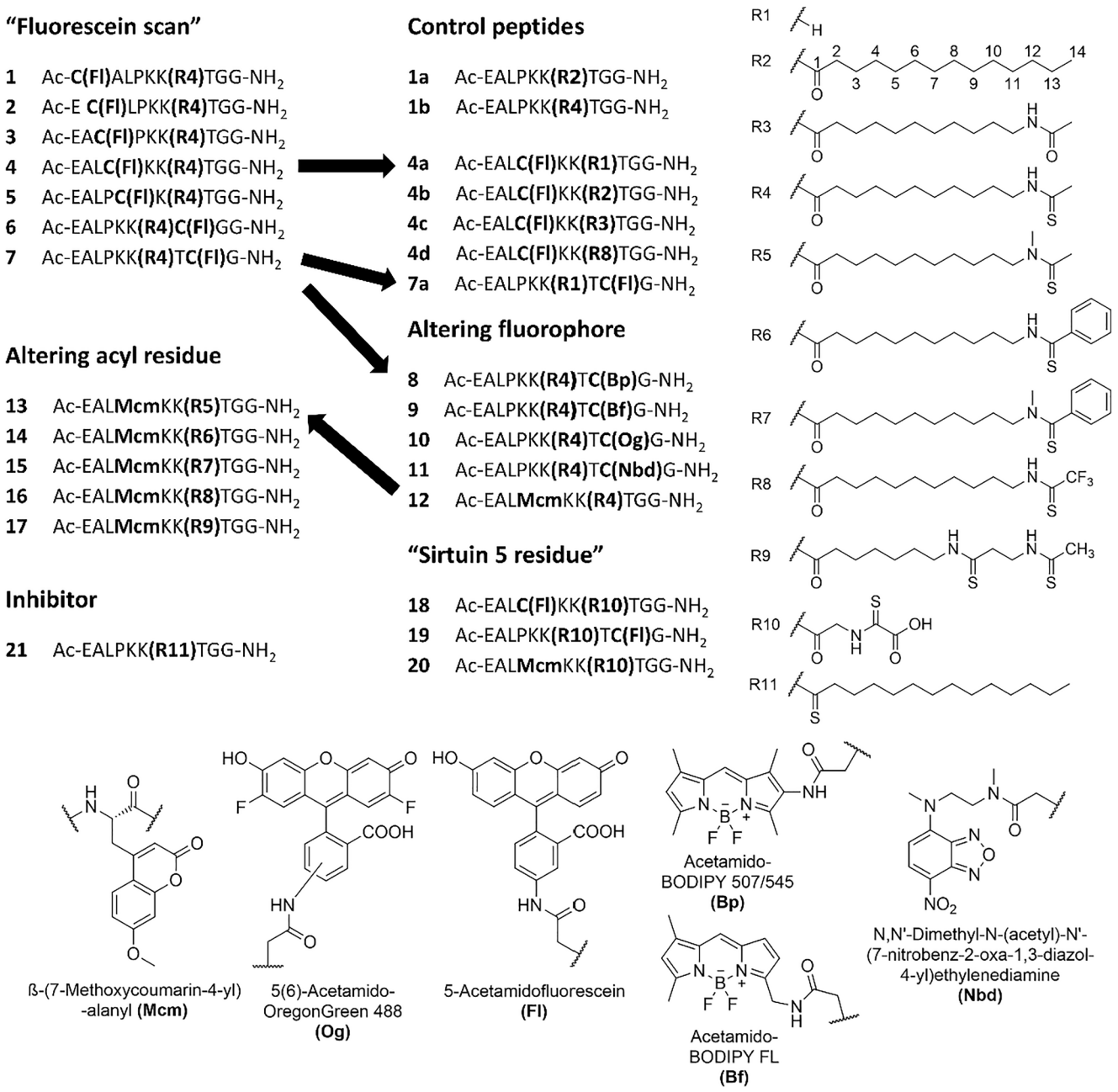

Fig. 2. Overview of the peptide derivatives used in this work. The peptide sequence is derived from TNFα (amino acids 15–22). The fluorophore was incorporated into the peptide backbone either via the cysteine side chain or as amino acid derivative Mcm. The acyl modification of the N^{ε}-amino group of the lysine residue is marked as R (right).

methylene units (7/8 and 12/13) by thioamide moieties in one acyl chain (Fig. 2, peptide **17**). We selected the 7/8 position for the second thioamide in order to create a selective substrate because we had evidence that only Sirt2, but no other sirtuins can accommodate this modification (Fig. S27). As shown in Table 1 the additional second thioamide PET quencher increases the quenching efficacy to 71%.

Efficiency of fluorescence quenching by a PET mechanism, is dependent on the redox potential of both fluorophore and quencher. Additionally, fluorophore and quencher have to be in van der Waals contact to allow dynamic quenching by molecular collisions. In the case of thioamides as PET quencher the fluorophore will be reduced and the thioamide oxidized [26]. Quenching takes place if the free energy of electron transfer is negative [26]. Small structural changes can influence the reduction potential of the fluorophore or the oxidation potential of the thioamide quencher. In a systematic investigation Bordwell *et al.* could show that the oxidation potential of thioamides could be fine-tuned by modification of both the residues at the nitrogen and the residues at the thiocarbonyl carbon [27]. Substitution at the nitrogen and replacement of a methyl residue by a phenyl residue at the thiocarbonyl carbon increased the oxidation potential [27]. Inspired by this work we analyzed similar substitutions at the PET quencher thioamide moiety in peptide **12** (Fig. 2) which has a quenching efficiency of 55%. Incorporation of a tertiary thioamide bond by methylation of the thioamide nitrogen (Fig. 2 peptide **13**) and replacement of the methyl residue at the thiocarbonyl carbon by a trifluoromethyl moiety (Fig. 2, peptide **16**) did not improve the quenching efficiency significantly. In contrast, quenching efficiency is much better (Table 1) if a thiobenzoyl residue is attached to the 11-aminoundecanoyl residue (Fig. 2 peptide **14**) or *N*-methylated 11-aminoundecanoyl residue at the lysine side chain (Fig. 2 peptide **15**).

Table 1
Quenching efficiency. Q_E is represented as mean of Q_E at 0.5 μM, 1 μM, 1.5 μM, 2.5 μM using a microtiter plate reader to have assay conditions.

compound	Fluorophore	Q_E (%)
1	Fl	46.9
2	Fl	35.7
3	Fl	47.6
4	Fl	43.5
4c	Fl	−2.2
4d	Fl	50.3
5	Fl	46.8
6	Fl	48.3
7	Fl	48.1
8	Bp	6.7[a]
9	Bf	24.1; 52.5[a]
10	Og	45.0
11	Nbd	12.2[a]
12	Mcm	55.1
13	Mcm	58.2
14	Mcm	75.6
15	Mcm	77.2
16	Mcm	57
17	Mcm	71 [a]
18	Fl	7.1 [a]
19	Fl	10.3 [a]
20	Mcm	60.7 [a]

[a] Q_E was determined as difference of fluorescence intensity of the peptide with and without lysine modification at emission maximum of the peptide without lysine modification.

Sirt5 is known to specifically hydrolyze malonylated, succinylated and glutarylated lysine residues [28–29]. Therefore, we incorporated a thioamide bond into the glutaryl residue resulting in peptides acylated with thiooxalylglycine (Fig. 2, peptides **18**–**20**). This modification is accepted by human Sirt5 resulting in substrates with k_{cat}/K_M-values in the range of 1000 $M^{-1}s^{-1}$ (data not shown). Unfortunately, the quenching efficacy of fluorescein fluorescence in either −2 (**18**) or +2 position (**19**) is suboptimal, which is presumably caused by the relatively rigid structure of the thioamide-containing acyl moiety preventing efficient van der Waals contact with the fluorophore. Switching to the coumarin fluorophore in the −2 position (**20**), we observed 60% quenching of the fluorescence.

Table 2 summarizes the results of our substrates **1**–**17** treated with HDAC11 or sirtuins 2,3,5, and 6. HDAC11 accepted all substrates with similar turnover (60–90% within one hour). Sirt6 also recognizes all compounds as substrates regardless of the fluorophore position but with significantly lower turnover compared to Sirt2 and Sirt3. No compound was found to be cleaved more effective through Sirt6 than the fluorescently labeled peptide with natural occurring myristoyl residue (**4b**). The highest conversion of the other compounds was seen of **4d** and **11**. Unfortunately, **11** is unusable for a fluorescence approach due to low quenching efficiency. Sirt2 and Sirt3 accept more or less all substrates with some preference for the fluorophore in the +2 position (**7**) and the −5 position (**1**), respectively. Also, the changes in the acyl residue (**12**–**16**) did not have a clear effect on the substrate preferences. Only compound **17** with two thioamide bonds in the acyl residue seems to be poorly recognized by Sirt3 and still accepted well by Sirt2. In contrast Sirt2 cleaves compound **7** very efficient with full substrate conversion after 1 h. To our surprise, Sirt5 was able to accept thioamide containing derivatives **1**–**7** with clear preferences for fluorescein in +2 positions (**7**). Changing the fluorophore at this position (**8**–**11**) has nearly no influence on the cleavage rate of Sirt5. Changing the fluorophore at another position (**12**) and the acyl residue (**13**–**17**) the substrate conversion remains low.

To analyze the substrate properties in more details, we determined the kinetic constants for HDAC11 and Sirt2, 3 and 5 using a microtiter plate fluorescence reader (Table 3). HDAC11 accepts the substrates of the "fluorescein scan" (**1**–**7**) with k_{cat}/K_M-values between 13,400 $M^{-1}s^{-1}$ and 51,000 $M^{-1}s^{-1}$. The specificity constants for **4** is about 4–5-fold higher compared to the continuous activity assay based on the same peptide sequence with the 2-aminobenzoylated 11-aminoundecanoyl residue (Fig. 1C) [9] and more than 8-fold higher as compared to a continuous substrate with the thiomyristoyl residue (Fig. 1F) [3]. Changing the fluorophore in +2 from fluorescein to BODIPY FL (**9**) furtherly improves the specificity constant, yielding the most efficient substrate for continuous HDAC11 activity measurements to date. Additionally, this specificity constant is 2.3-fold higher as compared to the myristoylated TNFα-substrate without any fluorophore [3]. As expected from the turnover measurements (Table 2), Sirt3 showed high specificity constants for substrates **1** and **7** with k_{cat}/K_M-values of 79,000 $M^{-1}s^{-1}$ and 36,000 $M^{-1}s^{-1}$, respectively. The value for **1** is about 28-fold higher as compared to the continuous activity assay based on a very similar peptide sequence with the 2-aminobenzoylated 11-aminoundecanoyl residue (Fig. 1C) [8]. The substrate properties of **7** and **9** for Sirt5 are remarkable. Fluorophores in the + 2 position are accepted, resulting in specificity constants between 280 $M^{-1}s^{-1}$ and 420 $M^{-1}s^{-1}$, respectively. These values are much higher than values reported for non-negatively charged, acetylated substrates like acetylated CPS-1 derived substrate with k_{cat}/K_M-value 16 $M^{-1}s^{-1}$ [30].

Inspection of the data presented in Table 3 revealed that thioacylated 11-aminoundecanoyl residues in combination with fluorophores in the peptide sequence yielded "super-substrates" for Sirt2 mainly based on extremely low K_M-values. To our knowledge, resulting specificity constants between 6,800,000 $M^{-1}s^{-1}$ for **7** and 15,000,000 $M^{-1}s^{-1}$ for **14** represent values never reported so far for any sirtuin. Inspection of kinetic constants for **12** and **13** shows that *N*-methylation of the thioamide moiety has nearly no influence on recognition by HDAC11 or Sirt2. Additionally, substitution of the thioacetyl moiety in **12** and **13** by the more bulky and more hydrophobic thiobenzoyl residues (**14** and **15**, respectively) results in nearly five-fold better substrates for Sirt2 but not for HDAC11 (Table 3) pointing to differences in the recognition of the hydrophobic acyl chain by the enzymes. This can be explained by the high complementarity of obtained substrates with the Sirt2 substrate binding pocket. Molecular modeling showed that the amino acid residues of the substrates are making multiple hydrogen bonds at the

Table 2
Substrate properties of peptide derivatives 1–20 for HDAC11 and different sirtuin isoforms. Data are represented in % of product formation (n = 3) subsequent to treatment with 50 nM HDAC11, 0.1 μM Sirt2, 0.1 μM Sirt3, 0.5 μM Sirt5, and 0.5 μM Sirt6, for 1 h at 37 °C. 0 means product formation < 0.2%. Graphical representation and additional 3 h timepoint are available in supporting information (Fig. S29-S30, Table S3).

compound	HDAC11	Sirt2	Sirt3	Sirt5	Sirt6
1	86 ± 4	60 ± 10	42 ± 4	1.7 ± 0.4	15 ± 1
1b	78 ± 4	16 ± 1	39 ± 1	29 ± 2	10 ± 1
2	84 ± 8	46 ± 3	28 ± 4	1.4 ± 0.5	17 ± 1
3	86 ± 3	43 ± 1	14 ± 1	1 ± 0.1	7.9 ± 0.4
4	89 ± 1	51 ± 7	10 ± 2	3.4 ± 0.6	9.3 ± 0.6
4b	67 ± 6	47 ± 5	46 ± 10	18 ± 3	31 ± 2
4c	69 ± 3	92 ± 5	6 ± 1	1.5 ± 0.1	9.8 ± 1.0
4d	80 ± 5	69 ± 1	29 ± 6	7.4 ± 1.3	22 ± 3
5	64 ± 5	53 ± 4	13 ± 2	1.1 ± 0.2	4.0 ± 0.1
6	81 ± 4	43 ± 6	12 ± 2	3.7 ± 0.6	11 ± 1
7	81 ± 11	100 ± 1	35 ± 5	26 ± 2	11 ± 2
8	83 ± 6	16 ± 1	41 ± 3	27 ± 2	11 ± 2
9	76 ± 7	29 ± 2	21 ± 2	24 ± 2	8.6 ± 2.0
10	84 ± 3	61 ± 4	36 ± 4	19 ± 2	7.7 ± 0.9
11	55 ± 2	16 ± 1	32 ± 1	40 ± 3	25 ± 2
12	89 ± 3	55 ± 5	17 ± 3	3 ± 1	7.6 ± 0.8
13	92 ± 1	69 ± 10	17 ± 2	1.2 ± 0.1	9.4 ± 0.9
14	79 ± 19	60 ± 7	14 ± 3	2.3 ± 0.5	6.7 ± 2.4
15	84 ± 1	50 ± 4	16 ± 3	1.7 ± 0.1	8.8 ± 0.5
16	56 ± 3	52 ± 3	19 ± 3	4.7 ± 0.1	12.6 ± 1.3
17	–	68 ± 5	4 ± 0.4	0.4 ± 0.03	2.4 ± 0.2
18	–	0	0	6.9 ± 0.1	0
19	–	10 ± 1	9.1 ± 0.2	7.3 ± 0.5	0
20	–	1.1 ± 0.2	0.20 ± 0.02	4 ± 0.2	0

Table 3
Kinetic parameters for HDAC11 and different sirtuin isoforms measured with Platereader with fluorescence readout, HPLC or fluorescence spectrometer. Concentrations of enzyme used in the assay are shown in parentheses below the enzyme name. Data are represented as mean of 3 independent replicates ± standard deviation. v/[S] plots could be observed in the supporting information (Fig. S31 – Fig. S37).

Enzyme	Cmpd	K_M (μM)	k_{cat} (s^{-1})	k_{cat}/K_M ($s^{-1}M^{-1}$)
HDAC11 (10–20 nM)	**1**	8.2 ± 0.5	0.22 ± 0.01	2.7×10^4
	1[*]	9.2 ± 2.6	0.34 ± 0.01	3.6×10^4
	2	13 ± 2	0.25 ± 0.03	1.9×10^4
	3	24 ± 3	0.59 ± 0.04	2.5×10^4
	4	5.7 ± 1.5	0.29 ± 0.02	5.1×10^4
	4[*]	5.8 ± 2.6	0.37 ± 0.01	6.7×10^4
	5	16 ± 2	0.22 ± 0.02	1.3×10^4
	5[*]	13 ± 1	0.15 ± 0.01	1.1×10^4
	6	22 ± 2	0.4 ± 0.05	1.8×10^4
	7	14 ± 3	0.25 ± 0.04	2.7×10^4
	9	5.8 ± 0.1	0.47 ± 0.03	8.1×10^4
	10	13 ± 2	0.23 ± 0.03	1.8×10^4
	12	9.5 ± 0.8	0.26 ± 0.04	2.7×10^4
	13	3.4 ± 0.2	0.089 ± 0.017	2.6×10^4
	14	3.9 ± 0.9	0.10 ± 0.02	2.6×10^4
	15	2.6 ± 0.3	0.049 ± 0.003	1.9×10^4
Sirt2 (0.5–2 nM)	**1**	0.010 ± 0.001	0.011 ± 0.002	1.1×10^6
	2	0.014 ± 0.001	0.0099 ± 0.0004	7.1×10^5
	3	0.010 ± 0.002	0.013 ± 0.001	1.3×10^6
	4	0.015 ± 0.002	0.014 ± 0.003	9.4×10^5
	4d	0.0058 ± 0.0003	0.0063 ± 0.001	1.1×10^6
	5	0.054 ± 0.006	0.013 ± 0.002	2.4×10^5
	6	0.035 ± 0.004	0.011 ± 0.001	2.9×10^5
	7	0.0053 ± 0.001	0.036 ± 0.007	6.8×10^6
	10	0.010 ± 0.001	0.016 ± 0.003	1.6×10^6
	12[a]	0.0061 ± 0.0003	0.019 ± 0.001	3.0×10^6
	13[a]	0.0044 ± 0.0004	0.012 ± 0.002	2.7×10^6
	14[a]	0.0011 ± 0.0001	0.017 ± 0.002	15×10^6
	15[a]	0.0012 ± 0.0002	0.016 ± 0.003	13×10^6
	16[a]	0.0015 ± 0.0003	0.010 ± 0.001	6.4×10^6
Sirt3 (10–20 nM)	**1**	0.28 ± 0.01	0.022 ± 0.003	7.9×10^4
	7	0.56 ± 0.01	0.020 ± 0.003	3.6×10^4
	10	1.4 ± 0.3	0.027 ± 0.001	2.0×10^4
Sirt5 (0.5 μM)	**7**	2 ± 0.2	$7.1 \times 10^{-4} \pm 0.6 \times 10^{-4}$	3.5×10^2
	9	19 ± 3	$7.9 \times 10^{-3} \pm 1.4 \times 10^{-3}$	4.2×10^2
	10	12 ± 1	$3.3 \times 10^{-3} \pm 0.2 \times 10^{-3}$	2.8×10^2

[*] were measured using HPLC;
[a] measured using fluorescence spectrometer.

Table 4
IC_{50} values. IC_{50} values determined with 10 nM **7** and 500 pM Sirt2, 0.27 μM **1** and 10 nM Sirt3, 2 μM **7** and 0.5 μM Sirt5 and 2 μM **4** and 5 nM HDAC11. Data are represented as mean of 3 independent replicated ± standard deviation. Dose response curves of IC_{50} determination could be observed in the supporting information (Fig. S54 – Fig. S57).

Enzyme	Compound	IC_{50} (μM) ± SD (n = 3)	IC_{50} (μM) reported
Sirt2	S2i5L	0.048 ± 0.007	0.013 [32], 1.2[a] [8]
	SirReal2	1.3 ± 0.1	0.4 [31]
	SirReal2 (K_i)	0.68	0.22 [31]
Sirt3	NAM	198 ± 31	377 [33], 186[a] [8]
	3-Typ	168 ± 4	38 [33]
Sirt5	DK5.1	3.5 ± 0.8	1.6 [34]
	NAM	210 ± 30	700 [35]
HDAC11	Trichostatin A (TSA)	2.6 ± 0.3	0.014 [36], 0.017 [37], 0.025 [38], 0.031 [39], 0.015 [40], 32 [6], 10 [9], 22 [9]
	Panobinostat (LBH-589)	0.37 ± 0.03	4.4 [27186676]
	Quisinostat (JNJ-26481585)	0.53 ± 0.23	0.37 [41], 3.3 [9], 1.8 [9]
	CUDC-907 (Fimepinostat)	0.040 ± 0.014	0.023 [9], 0.016 [9], 0.0054 [42]

[a] calculated from K_i value.

entrance to the substrate binding pocket similar to the co-crystallized peptide. Meanwhile, the long thioacylated 11-aminoundecanoyl lysine residue is placed comfortably in the hydrophobic Sirt2 substrate binding pocket (Fig. 3A). Its scissile amide bond interacts with valine 233 and in the absence of the co-substrate is stabilized by a water molecule. The benzoyl substituent of **14** is embedded into the aromatic cage at the end of the pocket formed by amino acid residues Y139, F143 and F190. Interestingly, this aromatic cage is not observed in the substrate-bound conformation of Sirt3 (Fig. 3B) despite presence of the aromatic amino acid residues at the corresponding positions of the amino acid sequence (Y200, Y204 and F251). The hydrophobic acyl-lysine residues of the substrates point to the allosteric pocket and the benzoyl group of **14** is located near the solvent exposed exit of the tunnel surrounded by non-aromatic residues T150, P155 and D156.

As expected from the results of the "thioamide scan" **17** represents a good substrate for Sirt2 but is not accepted by Sirt3, Sirt5 and Sirt6 (Fig. S27).

We recorded the absorbance spectra for **4a**, **4**, and **4d** and found remarkable differences in the range of 490–502 nm (Fig. S38). In principle these differences are sufficient to monitor sirtuin and HDAC11 activity following absorption at 490 nm (Fig. S38-S41). Fig. 4A shows the fluorescence spectra of **4**, **4a** and **4c**. Fluorescence intensity is much lower for **4** as compared to **4a** and the quenching is dependent on the presence of the thioamide moiety. If the thioamide is replaced by an amide bond (**4c**) resulting fluorescence is similar to **4a**. The observed difference in fluorescence for the substrate and the peptidic cleavage product of the sirtuin reaction enabled recording of progress curves as demonstrated in Fig. 4B for substrate **7** in the presence of different concentrations of Sirt2. In control experiments no significant change in the fluorescence signal over time could be observed either without NAD^+ in the presence of sirtuin or without sirtuin in the presence of NAD^+ (Fig. S42). This indicated that the observed fluorescence change results directly from sirtuin-mediated deacylation and not from unspecific interactions between NAD^+ and/or Sirt2 and **7**. The slope of the fluorescence increase at 535 nm is dependent on the enzyme concentration resulting in a linear correlation between Sirt2 amount and the reaction rate (Fig. 4C). We used a completely converted assay solution (controlled by LC-MS) for the generation of appropriate calibration curves (Fig. S43-S47). Based on the superior properties of substrate **7** we were able to monitor Sirt2 activity down to 0.1 nM concentration (Fig. 4C). Nevertheless, at such low concentrations of enzyme we had to include blocking reagents like bovine serum albumin (BSA) to the reaction solution in order to avoid unspecific binding and inactivation of enzyme and the peptides to the surface of the microtiter plate wells. Fig. 4D summarizes deacylation of substrate **7** by SIRT2 in in buffers with increasing BSA concentrations. There, we found no sirtuin activity in the absence of BSA for Sirt2 (Fig. 4D) or Sirt3 (Fig. S48). Overall enzymatic activity is increased stepwise until BSA concentration of 1.3 mg/ml and reached a plateau at 2–3 mg/ml. Similar effects were observed for HDAC11 in previous work, where HDAC11 showed little or no enzyme activity without BSA in the buffer [9].

We measured Sirt2 activity at different concentrations of **7** in 96-, 384-, and 1536-well formats (Fig. 5A) in order to demonstrate the applicability of our newly developed assay to evaluate inhibitor efficacy in high-throughput screening campaigns. The resulting kinetic constants

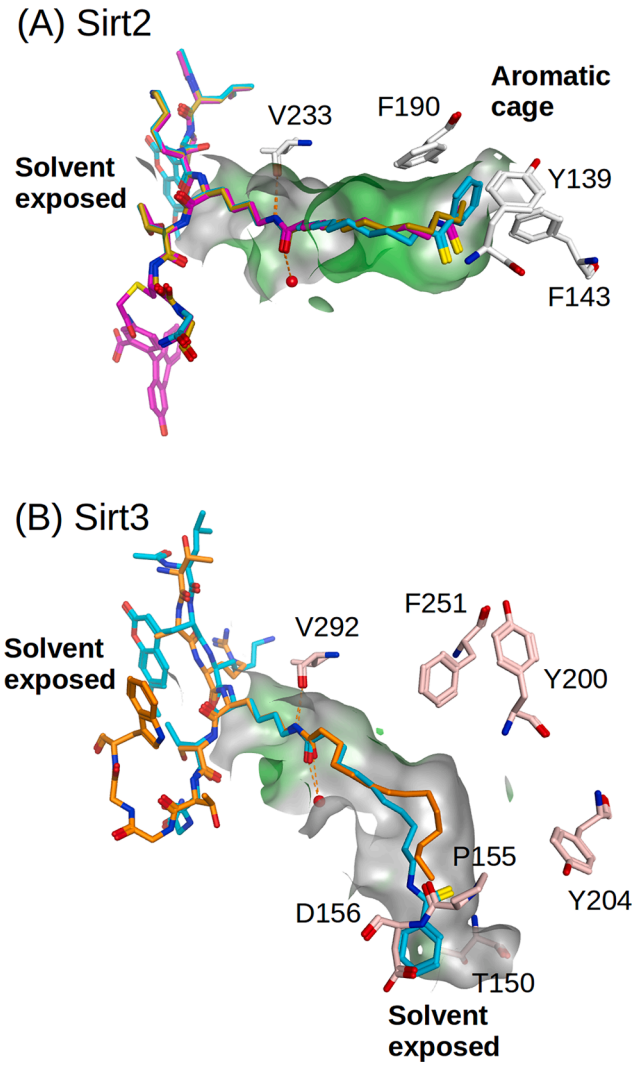

Fig. 3. Binding modes of peptide substrates 7 and 14 in Sirt2 PDB ID 4Y6O (**A**) and Sirt3 PDB ID 5BWN (**B**) derived from the docking study. The surface of the substrate binding pocket is colored green for hydrophobic areas and gray for neutral and hydrophilic zones. Relevant amino acid residues of the proteins are shown in stick representation and colored white for Sirt2 and pale pink for Sirt3. Peptide substrates are shown in stick representation with carbon atoms colored as followed: **7** – magenta, **14** – cyan, substrate co-crystallized with Sirt2 – mustard, peptide substrate co-crystallized with Sirt3 – orange. Heteroatoms are colored in a standard way: oxygen – red, nitrogen – blue, sulfur – yellow. Water molecule interacting with the scissile amide bond of the substrate is shown as a red ball. (For interpretation of the references to color in this figure legend, the reader is referred to the web version of this article.)

are comparable and the excellent statistical parameters of the assay Z′ factor between 0.90 and 0.88 (and S/N ratio between 75 and 177) confirmed the high-throughput potential of the HDAC11/Sirt2 activity measurements (Fig. 5, Fig. S49-52, Table S4). Next, we profiled the inhibitory potencies of several known Sirt2 inhibitors, including SirReal2 [31] and the cyclic peptide derivative S2i5L [32], using **7** as the substrate. SirReal2 is competitive against the peptide substrate (Fig. 5B) with a K_i-value of 0.68 μM (Fig. 5C) which is in good agreement with the reported value of 0.22 μM [31]. Moreover, we examined inhibitory activity of compounds Trichostatin A (TSA), CUDC-907, Quisinostat, and Panobinostat against HDAC11 using substrate **4** in a 96-well format (Fig. 5D). Again, the determined IC_{50} values correlate well with values determined using a different fluorescence-based and continuous HDAC11 activity assay [9].

Thiomyristoylated peptide derivatives represent effective Sirt2 inhibitors caused by the formation of a stalled intermediate reminiscent of a bisubstrate-analog inhibitor. The K_i value of thiomyristoylated TNFα derived peptide **21** (Fig. 2) is 80 nM if the enzymatic reaction is started with Sirt2 [8]. Using the substrate **7** we obtained biphasic progress curves resembling slow-binding inhibition yielding IC_{50} values of 4.3 ± 0.6 and 0.9 ± 0.1 nM using either the first phase or the slower phase for calculation, respectively (Fig. S53). In order to determine the IC_{50} value starting off the preformed stalled intermediate we pre-incubated 250 pM Sirt2 with **21** and NAD^+ for 15 min. Starting the enzymatic reaction by adding **7** yielded linear progress curves and enabled us to determine an IC_{50} value of 180 ± 20 pM for the stalled intermediate (Fig. S53B). This value is very close to half-concentration of Sirt2 allowing the speculation, that the assay conditions are still limiting and that the "real" IC_{50} value for the stalled intermediate formed by **21** and ADP-ribose is lower than 180 pM.

If the quenching of the fluorescence is caused by a PET mechanism, the substrates have to be conformationally flexible to allow for the necessary van der Waals contact between the thioamide moiety and the excited fluorophore. On the other hand, quenching via PET should not be possible if the substrate is bound to the active site of Sirt2 due to the spatial separation of the thioamide group and the fluorophore (Fig. 3A). Therefore, we monitored fluorescence intensity of 10 nM **7** in the presence of increasing amounts of Sirt2 (up to 2 μM resulting in 200-fold excess of the enzyme over the substrate). Fig. 6A shows a clear increase in fluorescence depending on the enzyme concentration resembling a titration curve with an inflection point at about 12 nM which is very close to the K_M value of **7**. This observation encouraged us to develop a fluorescent indicator displacement assay for Sirt2. Using a preformed complex of 250 nM Sirt2 and 10 nM of **7** (25-fold excess of Sirt2) we were able to determine a competitive displacement value of 6.8 μM for SirReal2 (Fig. 6B). Using an alternative readout, we were able to show that the change in fluorescence polarization could be used too for determination of binding of **7** to Sirt2 (Fig. 6C) resulting in a similar inflection point like in the fluorescence intensity readout.

3. Discussion

Detection of sirtuin and HDAC activity is often coupled to a separation step enabling independent quantification of a peptidic substrate and a product. Separation methods are different, including capillary electrophoresis [43], microchip electrophoresis [44], microfluidic mobility [45–46], polyacrylamide gel electrophoresis [47], high-performance liquid chromatography [28,48–50], thin layer chromatography [51], charcoal binding [52], binding to boronic acid resins [53] and extraction with organic solvents [54]. Nevertheless, the resulting assay format is discontinuous and therefore not suited for high-throughput applications. Alternatively, mass spectrometry allows quantification of peptidic substrates and products subsequent to separation in the gas phase [35,55–57]. MALDI-MS readout in combination with peptide derivatives immobilized on glass surfaces was used for the systematic profiling of the substrate specificity of Sirt1, Sirt3, HDAC2, HDAC3, and HDAC8 [58–59]. Additionally, sirtuin/HDAC activity patterns could be determined in cell lysates using that technique [60]. Alternative approaches make use of reagents and chemical reactions for sensing either the acetylated substrates, like acetyllysine-recognizing antibodies, [61–66] or the reaction products, like chemical reactions modifying the released primary amino function of the lysine side chain. Such reactions could be acylations with biotin-containing compounds or fluorescent dyes [67], alkylations with fluorescamine [68] or intramolecular reactions, like transesterification with a coumarin dye [69–71], or release of bioluminescent luciferin subsequent to an intramolecular cleavage of an ester bond [72] or intramolecular aldimine formation [73–74]. Additionally, spontaneous chromophore maturation after deacetylation of lysine 85 in enhanced green fluorescent protein enables monitoring of sirtuin activities in living cells via increase in fluorescence [75]. Using a similar approach, active site lysine 529 was

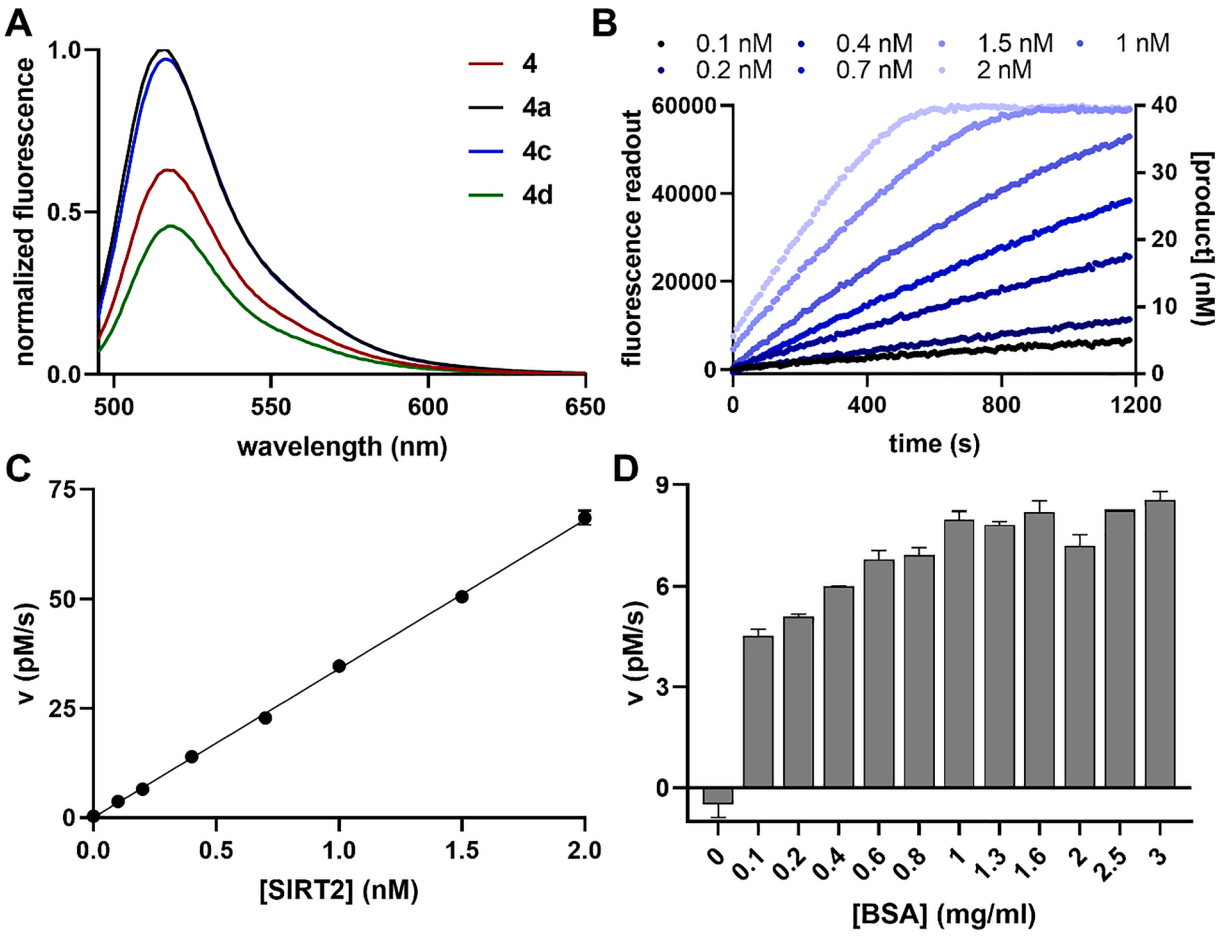

Fig. 4. A. Fluorescence spectra of **4a**, **4**, **4c**, **4d** at concentration of 1 μM. Excitation and emission wavelengths were set to 493 nm and 518 nm, respectively. **B.** Progress curves of Sirt2 mediated cleavage of **7** at 25 °C with 40 nM peptide, 500 μM NAD^+, and different SIRT2 concentrations ranging from 0.1 to 2 nM. Fluorescence readout was corrected by a negative control without enyzme. Product concentration was calculated using a calibration line (Fig S44). The excitation wavelength was set to 485 ± 14 nm and the emission wavelength to 35 ± 25 nm. **C.** Reaction rate of **7** from panel B is linearly dependent on the Sirt2-concentration at 40 nM substrate concentration. Error bars shows the standard deviation from triplicates of one experiment. **D.** Reaction rate of Sirt2 mediated cleavage of **7** as a function of BSA–concentration in the reaction mixture at 10 nM of **7** and a Sirt2 concentration of 250 pM.

replaced by acetylated lysine in firefly luciferase yielding an enzymatically inactive enzyme variant. Subsequent to treatment with different sirtuins deacetylation could be monitored in a continuous assay format by restored luciferase activity [76].

Alternatively, physical interactions of positively charged primary amino functions of lysine side chains with negatively charged molecules like DNA were used for monitoring of sirtuin/HDAC activity by aggregation-induced emission [77–78] and modulation of fluorescence properties [79–80].

It was demonstrated that substrates and products of sirtuin/HDAC reaction could be sensed by the coupling to enzymatic reactions either by using proteases, specific for the free lysine side chain of the peptidic product [48,81–83], by using combination of nicotinamidase/glutamate dehydrogenase for indirect spectrophotometric measurements of released nicotinamide [76] and by a cascade of enzymatic reactions to quantify the NAD^+ cosubstrate [46]. One advantage of monitoring the general product nicotinamide or the general cosubstrate NAD^+ is that it allows activity measurements independent of the nature of the peptide substrate. On the other hand, coupling the deacylase reaction to several enzymes makes the assay setup more complex, limits the linear range of the assay and makes the results more prone to artifacts caused by additional interaction of potential sirtuin/HDAC modulators with the coupling enzymes as demonstrated for the Sirt5 inhibitor GW5074 which affects enzymatic activity of the glutamate dehydrogenase [84].

Substrates used for protease coupled sirtuin/HDAC assays are often fused to substituted coumarins, generating bright fluorescence subsequent to cleavage of the lysyl-coumaryl amide bond [85–90]. Suboptimal proteolytic stability of different HDACs against the used proteases prohibited a continuous assay format, but there are reports for some sirtuins that this assay could be performed in a continuous manner [91–92].

Most of the published sirtuin assays have the limitation, that the substrate properties for the different sirtuin isoforms are suboptimal with regard to both, K_M and k_{cat} values, resulting in k_{cat}/K_M values in the range of 10–10,000 $M^{-1}s^{-1}$. This demands relatively high substrate concentrations and the low k_{cat} values lead to assay protocols with sirtuin concentrations in the range of 500 nM (Sirt2) up to 2 μM for Sirt6 measurements. Such settings limit the validity of the Michaelis-Menten equation and exacerbate correct determination of IC_{50} values for inhibitors binding with high affinity.

In contrast to most HDACs, sirtuins are able to accept longer acyl chains at the lysine side chain [4]. Based on this observation, three fluorescence based and continuous activity assays without any coupling to enzymatic or chemical reaction have been developed for sirtuins [8,10–11]. Subsequently, a similar assay was adapted to monitor HDAC11 activity [9]. In all cases, a fluorophore (or a quencher) is fused to the acyl moiety linked to the lysine side chain. Resulting substrates have good properties for Sirt2 and HDAC11 with k_{cat}/K_M values up to 175,000 $M^{-1}s^{-1}$ and 11,000 $M^{-1}s^{-1}$, respectively [8]. Recently, we were able to show that replacing the scissile bond by a thioamide bond is

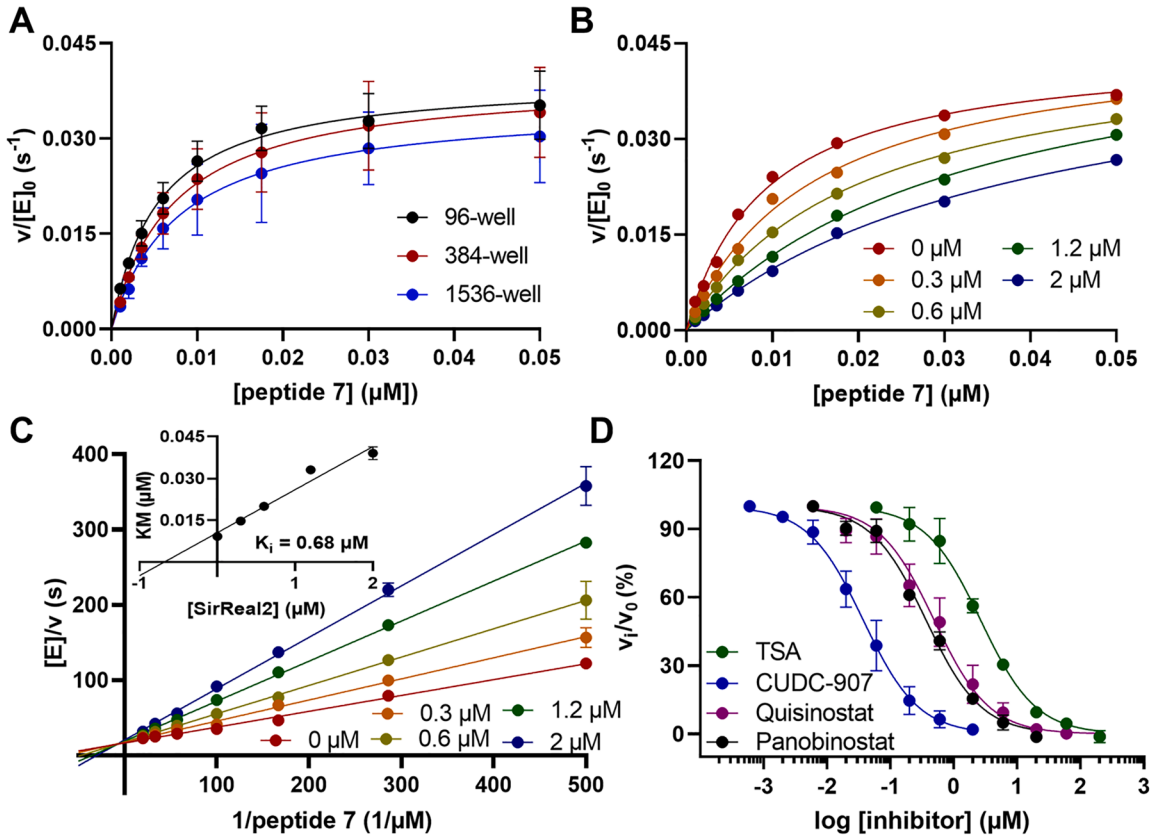

	96 well	384 well	1536 well
k_{cat} (s^{-1})	0.036	0.036	0.035
K_M (nM)	5.3	7.1	7.8
k_{cat}/K_M ($M^{-1} \cdot s^{-1}$)	6 800 000	5 100 000	4 500 000
Z‘ factor	0.90	0.89	0.88
S/N ratio	177	75	121

Fig. 5. A. v/[S] plots of 500 pM Sirt2 with different concentrations of **7** and 500 µM NAD^+ in three different well plate types. The resulting kinetic constants, the Z'-factor and the S/N ratio are summarized in the table under the figure. **B.** v/[S] plots of Sirt2 and **7** with different concentrations of the Sirt2 inhibitor SirReal2 with 500 pM Sirt2, 500 µM NAD^+ and altering concentrations of **7**. **C.** Lineweaver-Burk plot of the steady-state kinetics of **B,** showing a competitive binding mode of the inhibitor SirReal2, resulting in a K_i value of 0.68 µM. Hanes-Woolf plot and Dixon plot of the inhibitor measurement are shown in the supporting information (Fig. S52). **D.** Dose-response curves of four known HDAC11 inhibitors using 5 nM HDAC11 and 2 µM of **4**. The IC_{50} values are summarized in Table 4.

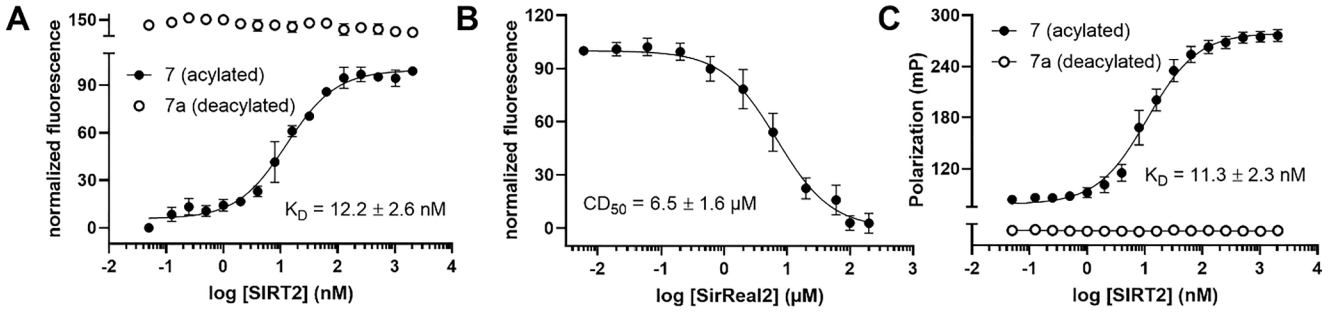

Fig. 6. A. Fluorescence change of 10 nM **7** or **7a** subsequent to treatment with increasing amount of Sirt2 (0.05 nM to 2048 nM) but without NAD^+. **B.** Binding curve of SirReal2 to Sirt2 generated by displacing **7** from Sirt2 which results in PET-based quenching of fluorescence intensity. The concentration of **7** was 10 nM and Sirt2 excess 25-fold (250 nM). **C.** Fluorescence polarization change of 10 nM **7** or **7a** subsequent to treatment with increasing amount of Sirt2 (0.05 nM to 2048 nM) but without NAD^+.

accepted by some HDAC isoforms yielding internally fluorescence-quenched HDAC8 super-substrates with k_{cat}/K_M values up to 450,000 $M^{-1}s^{-1}$. A similar replacement in sirtuin substrates is not productive because of the dramatically reduced substrate properties [20]. Therefore, we wondered if we could artificially introduce a thioamide bond into the fatty acid chain of myristoylated peptides (Fig. 2).

In combination with a respective fluorophore in the peptide chain the thioacylated 11-aminoundecanoylated lysine derivatives SIRT2 shows extremely low K_M values down to 5.3 nM for **7** and with further minor modifications at the acyl residue down to 1.1 nM (**14**). Known K_M values for continuous assay substrates for SIRT2 are 120 nM [8], 520 nM [10] and 41 nM recently shown by Nakajima *et al.* [11]. Compared with those substrates the K_M values for SIRT2 for substrates published in this study are more than 8 to 40 times lower. In contrast, the k_{cat} value with 0.36 s^{-1} (for SIRT2 and **7**) do not decrease significantly despite the low K_M values and is comparable to the published k_{cat} value (0.24 s^{-1}) for the aminobenzoylated 11-aminoundecanoyl substrate [8] yielded in a 85 fold increased k_{cat}/K_M value compared to this substrate.

Additionally, Sirt3, Sirt5 and Sirt6 are also able to recognize substrate **7**. Based on the low K_M value the "super-substrate" **7** allows measurements of the Sirt2 activity in a microtiter plate format with enzyme concentrations as low as 100 pM and substrate concentration of 10 nM. To the best of our knowledge this represents the most specific Sirt2 substrates described so far enabling highly effective microtiter plate-based inhibitor screening projects because of the reagent-saving and continuous nature of the assay format. Additionally, this substrate 7 represents a potential candidate for monitoring sirtuin 2 and HDAC11 activity in more complex biological fluids like cell lysates or within cells. Therefore, metabolic stability have to be increased because cleavages of peptide bonds between the fluorophore and the modified lysine residue by proteases will yield a fluorescence signal, too. One possibility is the replacement of single amino acid residues by either D-amino acids or *N*-methyl amino acids which are known to prevent proteolytic action. In a systematic study we were able to show that sirtuins can tolerate such modifications very well with the exception of the +1 position (data not shown). For cell-based experiments the metabolically stabilized substrate could be fused to oligo-arginines for better cell-penetration. We know that sirtuins recognize peptide substrate fused via the *N*-terminus to oligo(deca)-D-arginine (data not shown) opening the way of such substrates to be applied in living cells.

We could demonstrate that the underlying mechanism for substrate **7** is quenching by PET. Titrating **7** with Sirt2 in order to force **7** in an enzyme bound state increases the fluorescence up to a value of 70% fluorescence intensity of the corresponding peptide without PET Quencher (**7a**) or peptides derivatives having no PET quencher in their structure (**4c**). If the substrate **7** is bound to Sirt2 van der Waals contact between the thioamide bond and the fluorescein is not possible (Fig. 3A) preventing fluorescence quenching. Interestingly, this fluorescent substrate/enzyme complex could be used in a fluorescent indicator displacement assay format for fluorescence-based screening of inhibitors as demonstrated for the selective Sirt2 inhibitor SirReal2 (Fig. 6B).

In summary, we were able to demonstrate that fluorescence quenching by thioamides via a PET mechanism could be used for the development of highly efficient sirtuin and HDAC11 substrates which can be used for highly effective activity measurements using microtiter plate-based equipment. Moreover, PET mechanism allowed the development of an inhibitor screening based on either fluorescence polarization or fluorescent indicator displacement. Moreover, the developed substrates represent a starting point for the generation of probes enabling monitoring of sirtuin or HDAC11 activity in vivo.

4. Experimental section

4.1. Chemicals and general methods

All chemicals were purchased from Sigma-Aldrich (St. Louis, MO, USA) if not described otherwise. *N*,*N*-dimethylformamide (DMF), piperidine, ethyl(hydroxyamino)cyanoacetate (OxymaPure), pentafluorophenol, and Rink amide MBHA were purchased from Iris Biotech (Marktredwitz, Germany). 9-fluorenylmethoxy-carbonyl- (Fmoc) protected amino acid derivatives and O-(Benzotriazol-1-yl)-N,N,N′,N′-tetramethyluronium hexafluorophosphate (HBTU) were purchased from Merck (Darmstadt, Germany). Trifluoroacetic acid (TFA) was obtained from Roth (Karlsruhe, Germany). Fmoc-protected β-(7-methoxycoumarin-4-yl)-alanine (Mcm) was purchased from Bachem (Bubendorf, Switzerland). Fmoc-Lys(Ns)–OH, S2iL5 and DK5.1 were prepared as described before [8,34]. CUDC-907, JNJ-26481585 (Quisinostat), Panobinostat, 3-Typ, Trichostatin A and SirReal2 were purchased from Biomol (Hamburg, Germany). Fluorophores IANBD, 5-Iodoacetamidofluorescein, BODIPY 507/545-iodoacetamide, BODIPY-FL iodoacetamide, OregonGreen488 iodoacetamide (mixed isomers) were obtained from Thermo Fisher Scientific (Waltham, Massachusetts, USA).

For all HPLC analysis and purifications a system of water supplemented with 0.1% TFA (solvent A) and acetonitrile (ACN) supplemented with 0.1% TFA (solvent B) was used. Analytical runs were performed on an Agilent 1100 system (Boeblingen, Germany) with a quaternary pump, a well-plate autosampler and a diode array detector. Separation was done with a linear gradient from 5% to 95% solvent B within 6 min and a flowrate of 0.6 ml/min on a 3.0 × 50 mm reversed phase column (Phenomenex Kinetex XB C-18, 2.6 μm). Purification of peptides was done on Shimadzu LC System with a Phenomenex Kinetex™ 5 μm XB-C18 (250 × 21.1 mm, 100 Å) column using gradients ranging from 10% to 50% solvent B within 45 min to 25–80% solvent B.

UPLC-MS analysis was performed using either Waters Acquity UPLC-MS system or Waters XEVOTQD UPLC-MS system (Milford, USA) with a Waters Acquity-UPLC-MS-BEH C18; 1.7 μM (2.1 × 50 mm; 30 Å) column. As a mobile phase 0.1% formic acid in H_2O (solvent A) and 0.1% formic acid in ACN (solvent B) solutions were used. Typical gradient from 95:5 (v/v) of H_2O:ACN to 5:95 (v/v) of H_2O:ACN in 6 min was used for the most of the runs. Data analysis was performed using Waters MassLynx software.

4.2. Peptide synthesis

All Peptides were synthesized using an automated microwave peptide synthesizer Liberty Blue™ (CEM Corporation, Matthews, NC, USA) and Fmoc-based solid phase peptide synthesis (SPPS). The amino acid coupling was performed twice and with DIC/OxymaPure for 2 min at 90 °C. Fmoc deprotection was done with 20% piperidine solution in DMF for 1 min at 90 °C. *N*-terminal acetylation was performed with an acetic anhydride/DIPEA/DMF (1:2:7) mixture for 1 h at room temperature.

4.2.1. Modification of ε-amino group of lysine

Myristoyl modification was introduced via SPPS as Fmoc–Lys(Myr)–OH building block. Other modification of the ε-amino group of lysine were done on the resin after removal of 2-nitrobenzenesylfonyl (nosyl) group. Nosyl protecting group cleavage was done with a mixture of 1,8-diazabicyclo[5.4.0]undec-7-en (DBU)/thiophenol/DMF (1,5:1:7,5 v/v) (2 × 90 min). After washing with DMF, free lysine side chain was modified as described below. **1**–**12:** Resin was treated with Fmoc-11-aminoundecanoic acid (Fmoc-Aun-OH, 3 eq), HBTU (3 eq) and DIPEA (6 eq) in DMF for 1 h. After Fmoc deprotection (20% piperidine in DMF for 2 × 10 min) and washing (5 × 5 min with DMF), peptides were incubated with 4 eq of ethyl dithioacetate and 4 eq DIPEA in DMF for 1 h. **4a** and **7a:** nosyl protecting group was cleaved like described above. **4c:** After coupling of Fmoc-11-aminoundecanoic acid and Fmoc cleavage, peptide was incubated with an acetic anhydride/DIPEA/DMF (1:2:7) mixture for 1 h at room temperature. **4d** and **16:** After coupling of Fmoc-Aun-OH and Fmoc cleavage, resin was incubated with trifluorothioacetamide (5 eq) in DCM overnight. Then resin was incubated with a saturated solution of H_2S in tetrahydrofuran (THF) for 1 h. These

two steps were repeated once. **13**: After coupling of Fmoc-Aun-OH and Fmoc cleavage resin was incubated with 5 eq 2–nitrobenzenesylfonyl chloride and 10 eq 2,4,6-trimethylpyridine dissolved in *N*-methyl-2-pyrrolidone (NMP) for 15 min. After that, the resulted 2-nitrobenzenesulfonamide of Aun was methylated with triphenylphosphine (5 eq), methanol (MeOH, 10 eq) and diisopropyl azodicarboxylate (DIAD, 5 eq) in DMF for 2 × 30 min. The resin was incubated with 2–mercaptoethanol (10 eq) and DBU (5 eq) in DMF for 2 × 5 min. After washing with DMF resin was allowed to react with a solution of ethyl-dithioacetate (4 eq) and DIPEA (4 eq) overnight. **14:** After Fmoc-Aun-OH coupling and Fmoc-cleavage resin was incubated with S-(thiobenzoyl)thioglycolic acid (5 eq) and DIPEA (10 eq) overnight. **15**: After Fmoc-Aun-OH coupling and Fmoc-cleavage resin was incubated with 5 eq 2–nitrobenzenesylfonyl chloride and 10 eq 2,4,6-trimethylpyridine in NMP for 15 min. After that, the resulted nosylamide was methylated with triphenylphosphine (5 eq), MeOH (10 eq) and DIAD (5 eq) in DMF for 2 × 30 min. The resin was incubated with 2–mercaptoethanol (10 eq) and DBU (5 eq) in DMF for 2 × 5 min. After washing with DMF resin was incubated with S-(thiobenzoyl)thioglycolic acid (5 eq) and DIPEA (10 eq) overnight. **17:** After nosyl-group cleavage resin was treated with a solution of Fmoc-7-aminoheptanoic acid (4 eq), HBTU (4 eq) and DIPEA (8 eq) in DMF for 1 h, followed by Fmoc deprotection (20% piperidine in DMF, 2 × 10 min incubation) and washing 5 × 5 min with DCM. Then the resin was incubated with Fmoc-thio-β-alanyl-nitrobenztriazole (3 eq) and DIPEA (1 eq) in DCM for 1 h at room temperature followed by an Fmoc cleavage (20% piperidine in DMF, 2 × 10 min incubation) and washing 5 × 5 min with DCM. Afterwards the resin was incubated with 4 eq ethyl dithioacetate and 4 eq DIPEA for 1 h. **18**–**20**: After nosyl-group cleavage resin was incubated with Fmoc-glycine (4 eq), HBTU (4 eq) and DIPEA (8 eq) in DMF for 1 h followed by Fmoc cleavage (20% piperidine in DMF, 2 × 10 min incubation) and washing (5 × 5 min) with DCM. Then the resin was treated with *O-tert*-butyl-S-methyl-1,1-dithiooxalate (2 eq) dissolved in DCM for 1 h.

4.2.2. Global deprotection

After finishing synthesis on the resin, the resin was washed several times with DCM, then several times with MeOH and again with DCM. The resin was further incubated 2 times for 90 min in a H_2O/TFA/triisopropylsilane (TIPS) [95:2.5:2.5 (v/v/v)] and the volatiles were removed *in vacuo*. The residue was dissolved in a solution of ACN/H_2O [50:50 (v/v)], filtrated and purified with HPLC. Fractions containing the pure peptide (analyzed by UPLC-MS) were united, frozen, and lyophilized. The purity of the lyophilized material was determined with UPLC-MS.

4.2.3. Fluorophore coupling

12–17, 20: The Fmoc-ß-(7-Methoxy-coumarin-4-yl)-Ala-OH was introduced in the peptide backbone while standard SPPS and were ready for further usage after the first purification with HPLC. **1–11, 18, 19**: The lyophilized peptide was dissolved DMF and incubated with a solution of the appropriate fluorophore (0.67 eq) and DIPEA (6 eq) for 1 h at room temperature. After complete reaction (verified via UPLC-MS) solution was directly injected in the HPLC system and fraction with pure peptide were combined (judged by UPLC-MS), frozen and, lyophilized. Purity and identity was determined with UPLC-MS.

4.3. Cloning, expression and purification of recombinant enzymes

HDAC11 was cloned, expressed and purified as described [9]. All sirtuin genes were synthesized by Biocat GmbH. Human Sirt5 (34–302) was cloned with protease-cleavable *N*-terminal StrepII-tag [93] into pET-21a(+) vector. Sirt2 (43–356), Sirt3 (114–380) and Sirt6 (1–355 homolog 1) were cloned with protease-cleavable *N*-terminal StrepII-tag into pET-28a(+)-vector. All sirtuins were expressed in *E. coli* BL21 (DE3) in LB media supplemented with ampicillin or kanamycin, respectively. Overexpression was induced by the addition of IPTG in a final concentration of 0.5 mM at an OD600 of 0.6. Cells were harvested by centrifugation, resuspended in lysis buffer (100 mM Tris-HCl, 250 mM NaCl, 10 mM DTT, 1 mM EDTA, pH 8.0), and lysed by sonification. Cell debris was pelleted by ultracentrifugation and resulting supernatant was loaded onto a StrepTrap column (GE Healthcare, Uppsala, Sweden). The loaded column was intensively washed before elution with 5 mM desthiobiotin in 100 mM Tris, 250 mM NaCl, pH 8.0. Sirtuin-containing fractions were concentrated and finally separated using a Superdex 75 5/150 gel filtration column (GE Healthcare) equilibrated with 100 mM HEPES, 150 mM NaCl, 10 mM $CaCl_2$, 1 mM TCEP pH 7.8. All buffers for chromatographic steps were filtrated (0.22 μM) and degassed. Identity and homogeneity were finally confirmed via SDS-Page and LC-MS analysis as depicted in supplementary figures S58 and S59.

4.4. Fluorescence and UV-measurements

The UV measurements were done in a cuvette with an optical path length of 10 mm and a compound concentration 10 μM for peptides **1** to **11**, **18**, **19** and 30 μM for **12** to **17** and **20** at 25 °C in a M500 spectrophotometer (Carl Zeiss, Jena, Germany). The background absorbance of the appropriate buffer was subtracted from all spectra measured. The fluorescence spectra were recorded at a Fluoromax4 (Horiba, Kyōto, Japan) with a compound concentration of 1 μM at 25 °C. The excitation wavelength, excitation slits and emission slits are summarized in Table 5.

4.5. Determination of quenching efficiency

For determination of the quenching efficiency (Q_E) the peptides and the corresponding products were used. The product peptides were produces enzymatically with 50 μM peptide, 500 μM NAD^+ and 0.5 μM Sirt2 at 37 °C for 5 h. Full cleavage of peptides was confirmed with HPLC. The acylated peptides were treated in the same way but without enzyme. Q_E was determined in a black 96 well plate at 25 °C in a total volume of 100 μl at 0.5 μM, 1 μM, 1.5 μM and 2.5 μM final peptide concentration. Q_E was calculated with the following equation:

$$Q_E(\%) = 100\frac{product\ \ fluorescence - substrate\ \ fluorescence}{product\ \ fluorescence - backgroundfluorescence}$$

Background fluorescence is solution of Sirt2 and NAD^+ in buffer without peptide. The Q_E presented in Table 1 is the mean of Q_E at these 4 concentrations. Q_E for peptide 8, 9, 11, 17, 18, 19, 20 was determined using the fluorescence spectra (Fig. S60-S65) where the product fluorescence is the fluorescence intensity at λ_{max} of the peptide without acyl residue and the substrate fluorescence represents the fluorescence intensity of the peptide (with acyl residue) at the same wavelength.

4.6. HPLC-based deacylation assay

Reactions were performed in a total volume of 70 μl in Sirt-assay buffer containing 20 mM Tris-HCl (pH 7.8), 140 mM NaCl, 10 mM KCl and 2 mg/ml BSA for Sirt2, Sirt3, Sirt5 and Sirt6 or in HDAC11-assay buffer containing 20 mM of phosphoric acid (pH 7.4, adjusted with NaOH) and 2 mg/ml BSA for HDAC11. The peptides with a final concentration of 50 μM and 500 μM NAD^+ (only for sirtuins) were incubated for 5 min at 37 °C and the reaction was started with the addition of

Table 5
Settings for fluorescence measurements with Fluoromax 4.

Compound	λ_{Ex} (nm)	Exc slit (nm)	Em slit (nm)
1–7, 10, 18, 19	**492**	**0.5**	**2.5**
12–17, 20	**334**	**1**	**5**
8	**507**	**0.5**	**5**
9	**502**	**0.5**	**3.5**
11	**502**	**1**	**10**

enzyme ([HDAC11] = 50 nM, [Sirt2] = 100 nM, [Sirt3] = 100 nM, [Sirt5] = 500 nM and [Sirt6] = 500 nM final concentrations). After 1 h and after 3 h the reaction was quenched by addition of 1% TFA solution (final concentration at least 0.2%). Analysis of product formation was done with analytical HPLC. The quenched reaction solution was injected in the HPLC system (injection volume 40 µl) and compounds were separated with a linear gradient 5–95% solvent B in 6 min. Analysis of product peak area and substrate peak area were done with Agilent software Chemstation at 220 nm for **1b**, at 320 nm for **12**–**17** and **20**, at 450 nm for **1**–**7**, **9**, **10**, **18** and **19** and at 505 nm for **8** and **11**. Product formation was calculated as the ratio of product peak area to total peak area.

4.7. Steady state measurements

4.7.1. Plate reader

The kinetic measurements were carried out in black 96-well plate with flat bottom. The reaction take place in a total volume of 100 µl at 25 °C in HDAC11 assay buffer for HDAC11 and in Sirt-assay buffer for sirtuins (buffer composition as described above). For 384-well plate measurements a total volume of 20 µl and for 1536-well plates a total volume of 10 µl was used. Peptide substrates were dissolved in DMSO and the DMSO concentration was constant at 2% during the measurements. The peptide was incubated with 500 µM NAD^+ (only for sirtuins) in assay buffer for 5 min at 25 °C. The reaction was started with addition of enzyme. HDAC11 concentration was 10 nM for compounds **1** to **10** and 20 nM for **12**–**16** and peptide concentration varies between 0.25 µM and 20 µM. Sirt3 concentration was 20 nM and the peptide concentration varies between 0.05 and 3 µM. The Sirt5 concentration was 0.5 µM and the peptide concentration varies between 0.4 and 20 µM. The Sirt2 concentration was set to 0.25–2 nM depending on the peptide substrate and the peptide concentrations varies between 0.5 nM and 400 nM. The product formation was monitored via the fluorescence intensity, recorded by an Envision 2104 Multilabel Plate Reader (PerkinElmer, Waltham, MA). The filter settings for **1** to **10** was $\lambda_{Ex} = 485 \pm 14$ nm and $\lambda_{Em} = 535 \pm 25$ nm and for **12** to **16** $\lambda_{Ex} = 330 \pm 75$ nm and $\lambda_{Em} = 405 \pm 8$ nm. The fluorescence intensity was plotted vs. the time and the initial slope of these curves represents the reaction rate. The fluorescence intensity was transformed to product concentration using calibration lines as difference between substrate and product fluorescence (Fig. S43-S47). The reaction rate was plotted against the substrate concentration and a nonlinear regression according to the Michaelis-Menten equation was used to determine K_M and k_{cat} values using GraphPad Prism 8 software (San Diego, CA). For determination of kinetic constants K_M and k_{cat} of the HDAC11 reaction with **1**–**8** and **10** Hanes-Woolf plot was used.

4.7.2. HPLC

The peptide (and 500 µM NAD^+ for Sirt2) was preincubated in the appropriate assay buffer (see above) at different concentrations (0.5–40 µM HDAC11 and 0.25–4 µM Sirt2) for 5 min at 25 °C in 1.5 ml reaction vessel. The reaction was started with the addition of enzyme (3 nM final concentration). After different time points (5–40 min) the reactions was quenched with 1% TFA (final concentration at least 0.2%). The HPLC-method (injection, separation gradient, detection, and quantification) was like described above. Product concentration was plotted as a function of time and the initial slope of these curves represent the reaction rate. Determination of K_M and k_{cat} values was done like described above with the nonlinear regression according to the Michaelis-Menten equation.

4.7.3. Fluorescence spectrometer

The sensitivity of the Envision Multilabel Plate Reader in this setting was not high enough to determine the K_M and k_{cat} for Sirt2 and **12**–**16**. The fluorescence spectrometer was the alternative. All measurements were done in a fluorescence cuvette with 10 mm × 10 mm side length, at 25 °C in modified Sirt-assay buffer (20 mM Tris-HCl (pH 7.8), 140 mM NaCl, 10 mM KCl and 0.2 mg/ml BSA) at the Fluoromax4 (Horiba, Kyōto, Japan). The reaction solution with peptide (0.25–40 nM) and 500 µM NAD^+ was incubated at 25 °C in the cuvette for 5 min. The reaction started with the addition of Sirt2 (2 nM for **12**, **13**, **16** and 1 nM for **14** and **15** final concentration). The product formation was monitored with increase of fluorescence intensity at $\lambda_{Ex} = 334$ nm and $\lambda_{Em} = 397$ nm with an excitation/emission slit at 2/10 nm for **12**, **13** and **16** and with an excitation/emission slit at 2.5/20 nm for **14** and **15**. The fluorescence intensity was plotted against the time and the further determination of K_M and k_{cat} values were done as described in the "Plate Reader" section.

4.8. Determination of inhibition constants (IC_{50} values)

The IC_{50} values were determined in a black 96-well plate (Grainer Bio-One) in a total assay volume of 100 µl. For sirtuins the substrate was preincubated with altering concentrations of inhibitor and 0.5 mM NAD^+ in Sirt-assay buffer (as described above) at 25 °C for 5 min. The reaction was started with the addition of enzyme (10% of the total volume). Sirt2 was used with 10 nM of **7** and 500 pM of Sirt2 for SirReal2 and S2iL5 and 250 pM for compound **21**. Sirt3 was used with 0.27 µM **1** and 10 nM of Sirt3. Sirt5 was used with 0.5 µM Sirt5 and 2 µM of **7**. For HDAC11 the enzyme (5 nM final concentration) was incubated with different concentrations of inhibitor in HDAC11-assay buffer (as described above) and the reaction was started with the addition of compound **4** as substrate (final concentration 2 µM). The product formation was monitored with the increase of the fluorescence intensity at $\lambda_{Ex} = 485 \pm 14$ nm and $\lambda_{Em} = 535 \pm 25$ nm in a Perkin Elmer Envision plate reader. The initial rates of product formation were obtained from a linear regression of the plot fluorescence intensity as a function of time. The initial rates were normalized with the uninhibited reaction as 100% and the reaction without enzyme as 0%. The IC_{50} values were calculated with the following nonlinear equation for normalized reaction rates of a dose response curve in GraphPad Prism 8 software from a plot normalized activity as a function of logarithm of inhibitor concentration.

$$Y = \frac{100}{1 + 10^{X - logIC_{50}}}$$

4.9. Determination of Z' factor and S/N ratio

The Z' factor is a dimensionless statistical parameter to describe the quality of an HTS assay [94]. The Z' factor was calculated using the reaction rates of the Sirt2 deacylation reaction of **7** in different well plate types. The peptide concentration was chosen to be 10 nM like in the IC_{50} determination and 0.5 nM was the Sirt2 concentration. The fluorescence readout was done like described above (steady state measurements). The Z' factor was calculated with the following equation.

$$Z' = 1 - \frac{3SD100\% + 3SD0\%}{|mean_{100\%} - mean_{0\%}|}$$

$Mean_{100\%}$ was set as linear slope (reaction rate) of the reaction with 500 pM Sirt2, 500 µM NAD^+ and 10 nM **7** from a fluorescence intensity vs. time plot. $Mean_{0\%}$ is the negative control of this reaction without enzyme. The standard deviation of the reaction with enzyme (SD100%) and for the negative control (SD0%) was calculated with n = 3 (samples in one plate) for 96-well plate and with n = 4 (samples in one plate) for 384- and 1536-well plate. The Z' factor presented in this work is the mean of 3 independent assay repeats (Fig. S63).

The signal/noise ratio (S/N) was calculated with the values described above and the following equation [94]:

$$S/N = \frac{mean_{100\%} - mean_{0\%}}{SD_{0\%}}$$

4.10. Binding studies, fluorescence polarization and fluorescence indicator displacement assay

A serial dilution of Sirt2 in Sirt-assay buffer was done with final concentrations from 0.25 nM to 2000 nm Sirt2. **7** was added with a final concentration of 10 nM and then transferred to a black 384-well plate (small volume) with a total volume of 20 µl. The mixture was incubated for 10 min at 25 °C. The fluorescence readout was done with Envision 2104 Multilabel plate reader (PerkinElmer) with $\lambda_{Ex} = 485 \pm 14$ nm and $\lambda_{Em} = 535 \pm 25$ nm. The fluorescence intensity was normalized with **7** without Sirt2 as 0% and 2 µM Sirt2 with **7** was set to 100%. The fluorescence polarization readout was done with $\lambda_{Ex} = 485 \pm 14$ nm, $\lambda_{Em} = 535 \pm 40$ nm (S-pol) and $\lambda_{Em} = 535 \pm 40$ nm (P-pol) with the PerkinElmer 2104 Envision Multilabel plate reader and calculation for polarization was done with the device software WallacEnvision Manager. Fluorescence indicator displacement assay was started with a serial dilution of the Sirt2 inhibitor SirReal2 in 5% DMSO in Sirt-assay-buffer from 200 µM to 6 nM (final concentration). A mixture of 10 nM **7** and 250 nM Sirt2 (final concentration) was added to the inhibitor solution and transferred in a black 384-well plate and incubated for 10 min at 25 °C. Fluorescence readout was done like described above. The fluorescence was normalized with **7** without enzyme as 0% and **7** with Sirt2 but without inhibitor as 100%. Relative fluorescence was plotted as function of lg [inhibitor] and the CD_{50} was determined with the following nonlinear equation.

$$Y = \frac{Bottom + Top - Bottom}{1 + 10^{X - logCD_{50}}}$$

4.11. Computational studies

Sirt2 (PDB ID 4Y6O, [95] and Sirt3 (PDB ID 5BWN, [96] protein structures in complex with myristoylated peptides were downloaded from the Protein Data Bank rcsb.org [97]. The protein structures were prepared by using the Structure Preparation module in MOE2012.01 [98]. Hydrogen atoms were added, for titratable amino acids the protonation state was calculated using the Protonate 3D module in MOE. Protein structures were energy minimized using the AMBER99 force field [99] using a tethering force constant of (3/2) kT / 2 (σ = 0.5 Å) for all atoms during the minimization. AM1-BCC charges were used for the studied ligands. All molecules except the zinc ion were removed from the structures. Protein-ligand docking was performed using program GOLD5.8.1 [100]. His187 (Sirt2) and His248 (Sirt3) were used to define the size of the grid box (20 Å radius). 100 docking poses were calculated for the docked peptide substrates. To reduce the conformational sampling for the flexible peptide's hydrogen bonds observed between the co-crystallized peptides and Sirt2/3 in the X-ray structures were considered as protein H-bond constraints in GOLD. All other options were left at their default values. One conserved water molecule interacting with the scissile amide bond was considered as part of the protein for the docking. This protocol was correctly reproducing the binding mode of the reference peptides (taken from the Sirt2-peptide complex PDB ID 4Y6O and Sirt3-peptide complex PDB ID 5BWN) with heavy atom RMSD values below 2.5 Å.

Funding

This work was supported by grants from Deutsche Forschungsgemeinschaft (INST 271/336–1 FUGG) to M.S., the Czech Science Foundation (21-31806S to C.B.), the CAS (RVO: 86652036 to C.B.).

Declaration of Competing Interest

The authors declare that they have no known competing financial interests or personal relationships that could have appeared to influence the work reported in this paper.

Acknowledgments

The authors thank Ilona Kunze for excellent technical support. Moreover, the authors are grateful to Petra Baranova and Zsofia Kutil for HDAC11 production. The authors thank Prof. Dr. Thomas Kiefhaber at the Martin Luther University Halle-Wittenberg for giving access to the single-quadrupole LC-MS analyses and the core facility proteomic mass spectrometry of the Martin-Luther University Halle-Wittenberg for technical assistance during the triple-quadrupole LC-MS experiments.

Appendix A. Supplementary material

Supplementary data to this article can be found online at https://doi.org/10.1016/j.bioorg.2021.105425.

References

[1] B.C. Smith, W.C. Hallows, J.M. Denu, Mechanisms and molecular probes of sirtuins, Chem. Biol. 15 (10) (2008) 1002–1013, https://doi.org/10.1016/j.chembiol.2008.09.009.
[2] M. Schutkowski, F. Fischer, C. Roessler, C. Steegborn, New assays and approaches for discovery and design of Sirtuin modulators, Expert Opin. Drug Discov. 9 (2) (2014) 183–199, https://doi.org/10.1517/17460441.2014.875526.
[3] M. Zessin, Z. Kutil, M. Meleshin, Z. Nováková, E. Ghazy, D. Kalbas, M. Marek, C. Romier, W. Sippl, C. Bařinka, M. Schutkowski, One-atom substitution enables direct and continuous monitoring of histone deacylase activity, Biochemistry 58 (48) (2019) 4777–4789, https://doi.org/10.1021/acs.biochem.9b0078610.1021/acs.biochem.9b00786.s001.
[4] J.L. Feldman, J. Baeza, J.M. Denu, Activation of the protein deacetylase SIRT6 by long-chain fatty acids and widespread deacylation by mammalian sirtuins, J. Biol. Chem. 288 (43) (2013) 31350–31356, https://doi.org/10.1074/jbc.C113.511261.
[5] Z. Kutil, Z. Novakova, M. Meleshin, J. Mikesova, M. Schutkowski, C. Barinka, Histone deacetylase 11 is a fatty-acid deacylase, ACS Chem. Biol. 13 (3) (2018) 685–693, https://doi.org/10.1021/acschembio.7b0094210.1021/acschembio.7b00942.s00110.1021/acschembio.7b00942.s002.
[6] C. Moreno-Yruela, I. Galleano, A.S. Madsen, C.A. Olsen, Histone deacetylase 11 Is an ε-N-myristoyllysine hydrolase, cell, Chem. Biol. 25 (7) (2018) 849–856.e8, https://doi.org/10.1016/j.chembiol.2018.04.007.
[7] J.i. Cao, L. Sun, P. Aramsangtienchai, N.A. Spiegelman, X. Zhang, W. Huang, E. Seto, H. Lin, HDAC11 regulates type I interferon signaling through defatty-acylation of SHMT2, Proc. Natl. Acad. Sci. U. S. A. 116 (12) (2019) 5487–5492, https://doi.org/10.1073/pnas.1815365116.
[8] S. Schuster, C. Roessler, M. Meleshin, P. Zimmermann, Z. Simic, C. Kambach, C. Schiene-Fischer, C. Steegborn, M.O. Hottiger, M. Schutkowski, A continuous sirtuin activity assay without any coupling to enzymatic or chemical reactions, Sci. Rep. 6 (2016) 22643, https://doi.org/10.1038/srep22643.
[9] Z. Kutil, J. Mikešová, M. Zessin, M. Meleshin, Z. Nováková, G. Alquicer, A. Kozikowski, W. Sippl, C. Bařinka, M. Schutkowski, Continuous activity assay for HDAC11 enabling reevaluation of HDAC inhibitors, ACS Omega 4 (22) (2019) 19895–19904, https://doi.org/10.1021/acsomega.9b0280810.1021/acsomega.9b02808.s001.
[10] M. Kawaguchi, S. Ikegawa, N. Ieda, H. Nakagawa, A fluorescent probe for imaging sirtuin activity in living cells, based on one-step cleavage of the dabcyl quencher, Chembiochem 17 (20) (2016) 1961–1967, https://doi.org/10.1002/cbic.v17.2010.1002/cbic.201600374.
[11] Y. Nakajima, M. Kawaguchi, N. Ieda, H. Nakagawa, A set of highly sensitive sirtuin fluorescence probes for screening small-molecular sirtuin defatty-acylase inhibitors, ACS Med. Chem. Lett. 12 (4) (2021) 617–624, https://doi.org/10.1021/acsmedchemlett.1c0001010.1021/acsmedchemlett.1c00010.s001.
[12] E.J. Petersson, J.M. Goldberg, R.F. Wissner, On the use of thioamides as fluorescence quenching probes for tracking protein folding and stability, Phys. Chem. Chem. Phys. 16 (15) (2014) 6827–6837, https://doi.org/10.1039/C3CP55525A.
[13] J.M. Goldberg, S. Batjargal, E.J. Petersson, Thioamides as fluorescence quenching probes: minimalist chromophores to monitor protein dynamics, J. Am. Chem. Soc. 132 (42) (2010) 14718–14720, https://doi.org/10.1021/ja1044924.
[14] J.M. Goldberg, L.C. Speight, M.W. Fegley, E.J. Petersson, Minimalist probes for studying protein dynamics: thioamide quenching of selectively excitable fluorescent amino acids, J. Am. Chem. Soc. 134 (14) (2012) 6088–6091, https://doi.org/10.1021/ja3005094.
[15] J.M. Goldberg, S. Batjargal, B.S. Chen, E.J. Petersson, Thioamide quenching of fluorescent probes through photoinduced electron transfer: mechanistic studies and applications, J. Am. Chem. Soc. 135 (49) (2013) 18651–18658, https://doi.org/10.1021/ja409709x.
[16] J.M. Goldberg, X. Chen, N. Meinhardt, D.C. Greenbaum, E.J. Petersson, Thioamide-based fluorescent protease sensors, J. Am. Chem. Soc. 136 (5) (2014) 2086–2093, https://doi.org/10.1021/ja412297x.
[17] C. Liu, T.M. Barrett, X. Chen, J.J. Ferrie, E.J. Petersson, Fluorescent probes for studying thioamide positional effects on proteolysis reveal insight into resistance

to cysteine proteases, ChemBioChem 20 (16) (2019) 2059–2062, https://doi.org/10.1002/cbic.v20.1610.1002/cbic.201900115.
[18] J.M. Goldberg, R.F. Wissner, A.M. Klein, E.J. Petersson, Thioamide quenching of intrinsic protein fluorescence, Chem. Commun. 48 (10) (2012) 1550–1552, https://doi.org/10.1039/C1CC14708K.
[19] D.M. Robkis, E.M. Hoang, P. Po, C.J. Deutsch, E.J. Petersson, Side-chain thioamides as fluorescence quenching probes, Biopolymers 112 (1) (2021), https://doi.org/10.1002/bip.v112.110.1002/bip.23384.
[20] B.C. Smith, J.M. Denu, Mechanism-based inhibition of Sir2 deacetylases by thioacetyl-lysine peptide, Biochemistry 46 (50) (2007) 14478–14486, https://doi.org/10.1021/bi7013294.
[21] B. He, J. Hu, X. Zhang, H. Lin, Thiomyristoyl peptides as cell-permeable Sirt6 inhibitors, Org. Biomol. Chem. 12 (38) (2014) 7498–7502, https://doi.org/10.1039/C4OB00860J.
[22] H. Jing, J. Hu, B. He, Y.L. Negrón Abril, J. Stupinski, K. Weiser, M. Carbonaro, Y.-L. Chiang, T. Southard, P. Giannakakou, R.S. Weiss, H. Lin, A SIRT2-selective inhibitor promotes c-myc oncoprotein degradation and exhibits broad anticancer activity, Cancer Cell 29 (3) (2016) 297–310, https://doi.org/10.1016/j.ccell.2016.02.007.
[23] N.A. Spiegelman, J.Y. Hong, J. Hu, H. Jing, M. Wang, I.R. Price, J.i. Cao, M. Yang, X. Zhang, H. Lin, A small-molecule SIRT2 inhibitor that promotes K-Ras4a lysine fatty-acylation, ChemMedChem 14 (7) (2019) 744–748, https://doi.org/10.1002/cmdc.v14.710.1002/cmdc.201800715.
[24] H. Jiang, S. Khan, Y.i. Wang, G. Charron, B. He, C. Sebastian, J. Du, R. Kim, E. Ge, R. Mostoslavsky, H.C. Hang, Q. Hao, H. Lin, SIRT6 regulates TNF-α secretion through hydrolysis of long-chain fatty acyl lysine, Nature 496 (7443) (2013) 110–113, https://doi.org/10.1038/nature12038.
[25] Y.-B. Teng, H. Jing, P. Aramsangtienchai, B. He, S. Khan, J. Hu, H. Lin, Q. Hao, Efficient demyristoylase activity of SIRT2 revealed by kinetic and structural studies, Sci. Rep. 5 (2015) 8529, https://doi.org/10.1038/srep08529.
[26] J.V. Jun, D.M. Chenoweth, E.J. Petersson, Rational design of small molecule fluorescent probes for biological applications, Org. Biomol. Chem. 18 (30) (2020) 5747–5763, https://doi.org/10.1039/D0OB01131B.
[27] F.G. Bordwell, D.J. Algrim, J.A. Harrelson, The relative ease of removing a proton, a hydrogen atom, or an electron from carboxamides versus thiocarboxamides, J. Am. Chem. Soc. 110 (17) (1988) 5903–5904.
[28] J. Du, Y. Zhou, X. Su, J.J. Yu, S. Khan, H. Jiang, J. Kim, J. Woo, J.H. Kim, B. H. Choi, B. He, W. Chen, S. Zhang, R.A. Cerione, J. Auwerx, Q. Hao, H. Lin, Sirt5 is a NAD-dependent protein lysine demalonylase and desuccinylase, Science 334 (6057) (2011) 806–809, https://doi.org/10.1126/science:1207861.
[29] M. Tan, C. Peng, K. Anderson, P. Chhoy, Z. Xie, L. Dai, J. Park, Y. Chen, H. e. Huang, Y.i. Zhang, J. Ro, G. Wagner, M. Green, A. Madsen, J. Schmiesing, B. Peterson, G. Xu, O. Ilkayeva, M. Muehlbauer, T. Braulke, C. Mühlhausen, D. Backos, C. Olsen, P. McGuire, S. Pletcher, D. Lombard, M. Hirschey, Y. Zhao, Lysine glutarylation is a protein posttranslational modification regulated by SIRT5, Cell Metab. 19 (4) (2014) 605–617, https://doi.org/10.1016/j.cmet.2014.03.014.
[30] C. Roessler, T. Nowak, M. Pannek, M. Gertz, G.T.T. Nguyen, M. Scharfe, I. Born, W. Sippl, C. Steegborn, M. Schutkowski, Chemical probing of the human sirtuin 5 active site reveals its substrate acyl specificity and peptide-based inhibitors, Angew. Chem. Int. Ed Engl. 53 (40) (2014) 10728–10732, https://doi.org/10.1002/anie.201402679.
[31] T. Rumpf, M. Schiedel, B. Karaman, C. Roessler, B.J. North, A. Lehotzky, J. Oláh, K.I. Ladwein, K. Schmidtkunz, M. Gajer, M. Pannek, C. Steegborn, D.A. Sinclair, S. Gerhardt, J. Ovádi, M. Schutkowski, W. Sippl, O. Einsle, M. Jung, Selective Sirt2 inhibition by ligand-induced rearrangement of the active site, Nat. Commun. 6 (2015) 6263, https://doi.org/10.1038/ncomms7263.
[32] K. Yamagata, Y. Goto, H. Nishimasu, J. Morimoto, R. Ishitani, N. Dohmae, N. Takeda, R. Nagai, I. Komuro, H. Suga, O. Nureki, Structural basis for potent inhibition of SIRT2 deacetylase by a macrocyclic peptide inducing dynamic structural change, Structure 22 (2) (2014) 345–352, https://doi.org/10.1016/j.str.2013.12.001.
[33] U. Galli, O. Mesenzani, C. Coppo, G. Sorba, P.L. Canonico, G.C. Tron, A. A. Genazzani, Identification of a sirtuin 3 inhibitor that displays selectivity over sirtuin 1 and 2, Eur. J. Med. Chem. 55 (2012) 58–66, https://doi.org/10.1016/j.ejmech.2012.07.001.
[34] D. Kalbas, S. Liebscher, T. Nowak, M. Meleshin, M. Pannek, C. Popp, Z. Alhalabi, F. Bordusa, W. Sippl, C. Steegborn, M. Schutkowski, Potent and selective inhibitors of human sirtuin 5, J. Med. Chem. 61 (6) (2018) 2460–2471, https://doi.org/10.1021/acs.jmedchem.7b0164810.1021/acs.jmedchem.7b01648.s00110.1021/acs.jmedchem.7b01648.s002.
[35] F. Fischer, M. Gertz, B. Suenkel, M. Lakshminarasimhan, M. Schutkowski, C. Steegborn, P. Csermely, Sirt5 deacylation activities show differential sensitivities to nicotinamide inhibition, PLoS One 7 (9) (2012) e45098, https://doi.org/10.1371/journal.pone.004509810.1371/journal.pone.0045098.s00110.1371/journal.pone.0045098.s00210.1371/journal.pone.0045098.s00310.1371/journal.pone.0045098.s00410.1371/journal.pone.0045098.s00510.1371/journal.pone.0045098.s006.
[36] R. Neelarapu, D.L. Holzle, S. Velaparthi, H.e. Bai, M. Brunsteiner, S.Y. Blond, P. A. Petukhov, Design, synthesis, docking, and biological evaluation of novel diazide-containing isoxazole- and pyrazole-based histone deacetylase probes, J. Med. Chem. 54 (13) (2011) 4350–4364, https://doi.org/10.1021/jm2001025.
[37] C.-W. Yu, P.-T. Chang, L.-W. Hsin, J.-W. Chern, Quinazolin-4-one derivatives as selective histone deacetylase-6 inhibitors for the treatment of Alzheimer's disease, J. Med. Chem. 56 (17) (2013) 6775–6791, https://doi.org/10.1021/jm400564j.
[38] R. Muthyala, W.S. Shin, J. Xie, Y.Y. Sham, Discovery of 1-hydroxypyridine-2-thiones as selective histone deacetylase inhibitors and their potential application for treating leukemia, Bioorg. Med. Chem. Lett. 25 (19) (2015) 4320–4324, https://doi.org/10.1016/j.bmcl.2015.07.065.
[39] L. Marek, A. Hamacher, F.K. Hansen, K. Kuna, H. Gohlke, M.U. Kassack, T. Kurz, Histone deacetylase (HDAC) inhibitors with a novel connecting unit linker region reveal a selectivity profile for HDAC4 and HDAC5 with improved activity against chemoresistant cancer cells, J. Med. Chem. 56 (2) (2013) 427–436, https://doi.org/10.1021/jm301254q.
[40] R. Cincinelli, L. Musso, G. Giannini, V. Zuco, M. de Cesare, F. Zunino, S. Dallavalle, Influence of the adamantyl moiety on the activity of biphenylacrylohydroxamic acid-based HDAC inhibitors, Eur. J. Med. Chem. 79 (2014) 251–259, https://doi.org/10.1016/j.ejmech.2014.04.021.
[41] J. Arts, P. King, A. Mariën, W. Floren, A. Beliën, L. Janssen, I. Pilatte, B. Roux, L. Decrane, R. Gilissen, I. Hickson, V. Vreys, E. Cox, K. Bol, W. Talloen, I. Goris, L. Andries, M. Du Jardin, M. Janicot, M. Page, K. van Emelen, P. Angibaud, JNJ-26481585, a novel "second-generation" oral histone deacetylase inhibitor, shows broad-spectrum preclinical antitumoral activity, Clin. Cancer Res. 15 (22) (2009) 6841–6851, https://doi.org/10.1158/1078-0432.CCR-09-0547.
[42] Y. Chen, X. Wang, W. Xiang, L. He, M. Tang, F. Wang, T. Wang, Z. Yang, Y. Yi, H. Wang, T. Niu, L.i. Zheng, L. Lei, X. Li, H. Song, L. Chen, Development of purine-based hydroxamic acid derivatives: potent histone deacetylase inhibitors with marked in vitro and in vivo antitumor activities, J. Med. Chem. 59 (11) (2016) 5488–5504, https://doi.org/10.1021/acs.jmedchem.6b0057910.1021/acs.jmedchem.6b00579.s00110.1021/acs.jmedchem.6b00579.s002.
[43] Y.i. Fan, G.K.E. Scriba, Electrophoretically mediated microanalysis assay for sirtuin enzymes, Electrophoresis 31 (23-24) (2010) 3874–3880, https://doi.org/10.1002/elps.201000336.
[44] S. Ohla, R. Beyreiss, G.K.E. Scriba, Y. Fan, D. Belder, An integrated on-chip sirtuin assay, Electrophoresis 31 (2010) 3263–3267, https://doi.org/10.1002/elps.201000220.
[45] L. Blackwell, J. Norris, C.M. Suto, W.P. Janzen, The use of diversity profiling to characterize chemical modulators of the histone deacetylases, Life Sci. 82 (21-22) (2008) 1050–1058, https://doi.org/10.1016/j.lfs.2008.03.004.
[46] Y. Liu, R. Gerber, J. Wu, T. Tsuruda, J.D. McCarter, High-throughput assays for sirtuin enzymes: a microfluidic mobility shift assay and a bioluminescence assay, Anal. Biochem. 378 (1) (2008) 53–59, https://doi.org/10.1016/j.ab.2008.02.018.
[47] A.N. Khan, P.N. Lewis, Unstructured conformations are a substrate requirement for the Sir2 family of NAD-dependent protein deacetylases, J. Biol. Chem. 280 (43) (2005) 36073–36078, https://doi.org/10.1074/jbc.M508247200.
[48] P.A. Marcotte, P.L. Richardson, P.R. Richardson, J. Guo, L.W. Barrett, N. Xu, A. Gunasekera, K.B. Glaser, Fluorescence assay of SIRT protein deacetylases using an acetylated peptide substrate and a secondary trypsin reaction, Anal. Biochem. 332 (2004) 90–99, https://doi.org/10.1016/j.ab.2004.05.039.
[49] K.G. Tanner, J. Landry, R. Sternglanz, J.M. Denu, Silent information regulator 2 family of NAD- dependent histone/protein deacetylases generates a unique product, 1-O-acetyl-ADP-ribose, Proc. Natl. Acad. Sci. U. S. A. 97 (26) (2000) 14178–14182, https://doi.org/10.1073/pnas.250422697.
[50] M.D. Jackson, J.M. Denu, Structural identification of 2'- and 3'-O-acetyl-ADP-ribose as novel metabolites derived from the Sir2 family of beta -NAD+-dependent histone/protein deacetylases, J. Biol. Chem. 277 (2002) 18535–18544, https://doi.org/10.1074/jbc.M200671200.
[51] A.N. Khan, P.N. Lewis, Use of substrate analogs and mutagenesis to study substrate binding and catalysis in the Sir2 family of NAD-dependent protein deacetylases, J. Biol. Chem. 281 (17) (2006) 11702–11711, https://doi.org/10.1074/jbc.M511482200.
[52] M.T. Borra, J.M. Denu, Quantitative assays for characterization of the sir2 family of NAD+-dependent deacetylases, in: C.D. Allis, C. Wu (Eds.), Chromatin and chromatin remodeling enzymes: Part B, Elsevier Academic Press, Amsterdam, Boston, 2004, pp. 171–187.
[53] T. McDonagh, J. Hixon, P.S. DiStefano, R. Curtis, A.D. Napper, Microplate filtration assay for nicotinamide release from NAD using a boronic acid resin, Methods 36 (4) (2005) 346–350, https://doi.org/10.1016/j.ymeth.2005.03.005.
[54] K. Hoffmann, B. Heltweg, M. Jung, Improvement and validation of the fluorescence-based histone deacetylase assay using an internal standard, Arch. Pharm. Pharm. Med. Chem. 334 (2001) 248–252, https://doi.org/10.1002/1521-4184(200107)334:7<248:aid-ardp248>3.0.co;2-k.
[55] P.T. Rye, L.E. Frick, C.C. Ozbal, W.A. Lamarr, Advances in label-free screening approaches for studying sirtuin-mediated deacetylation, J. Biomol. Screen. 16 (10) (2011) 1217–1226, https://doi.org/10.1177/1087057111420291.
[56] S. Holzhauser, A. Freiwald, C. Weise, G. Multhaup, C.-T. Han, S. Sauer, Discovery and characterization of protein-modifying natural products by MALDI mass spectrometry reveal potent SIRT1 and p300 inhibitors, Angew. Chem. Int. Ed Engl. 52 (19) (2013) 5171–5174, https://doi.org/10.1002/anie.v52.1910.1002/anie.201207325.
[57] D.i. Shao, C. Yao, M.H. Kim, J. Fry, R.A. Cohen, C.E. Costello, R. Matsui, F. Seta, M.E. McComb, M.M. Bachschmid, Bachschmid, Improved mass spectrometry-based activity assay reveals oxidative and metabolic stress as sirtuin-1 regulators, Redox Biol. 22 (2019) 101150, https://doi.org/10.1016/j.redox.2019.101150.
[58] Z.A. Gurard-Levin, K.A. Kilian, J. Kim, K. Bähr, M. Mrksich, Peptide arrays identify isoform-selective substrates for profiling endogenous lysine deacetylase activity, ACS Chem. Biol. 5 (9) (2010) 863–873, https://doi.org/10.1021/cb100088g.
[59] Z.A. Gurard-Levin, J. Kim, M. Mrksich, Combining mass spectrometry and peptide arrays to profile the specificities of histone deacetylases, Chembiochem 10 (13)

(2009) 2159–2161, https://doi.org/10.1002/cbic.v10:1310.1002/cbic.200900417.
[60] H.-Y. Kuo, T.A. DeLuca, W.M. Miller, M. Mrksich, Profiling deacetylase activities in cell lysates with peptide arrays and SAMDI mass spectrometry, Anal. Chem. 85 (22) (2013) 10635–10642, https://doi.org/10.1021/ac402614x.
[61] Z. Kutil, L. Skultetyova, D. Rauh, M. Meleshin, I. Snajdr, Z. Novakova, J. Mikesova, J. Pavlicek, M. Hadzima, P. Baranova, B. Havlinova, P. Majer, M. Schutkowski, C. Barinka, The unraveling of substrate specificity of histone deacetylase 6 domains using acetylome peptide microarrays and peptide libraries, FASEB J. 33 (3) (2019) 4035–4045, https://doi.org/10.1096/fsb2.v33.310.1096/fj.201801680R.
[62] D. Rauh, F. Fischer, M. Gertz, M. Lakshminarasimhan, T. Bergbrede, F. Aladini, C. Kambach, C.F.W. Becker, J. Zerweck, M. Schutkowski, C. Steegborn, An acetylome peptide microarray reveals specificities and deacetylation substrates for all human sirtuin isoforms, Nat. Commun. 4 (2013) 2327, https://doi.org/10.1038/ncomms3327.
[63] M.B. Robers, C. Loh, C.B. Carlson, H. Yang, E.A. Frey, S.B. Hermanson, K. Bi, Measurement of the cellular deacetylase activity of SIRT1 on p53 via LanthaScreen® technology, Molecular bioSystems 7 (1) (2011) 59–66, https://doi.org/10.1039/C0MB00026D.
[64] J.M. Dudek, R.A. Horton, TR-FRET biochemical assays for detecting posttranslational modifications of p53, J. Biomol. Screen. 15 (5) (2010) 569–575, https://doi.org/10.1177/1087057110365898.
[65] T. Machleidt, M.B. Robers, S.B. Hermanson, J.M. Dudek, K. Bi, TR-FRET cellular assays for interrogating posttranslational modifications of histone H3, J. Biomol. Screen. 16 (10) (2011) 1236–1246, https://doi.org/10.1177/1087057111422943.
[66] F. Degorce, A. Card, S. Soh, E. Trinquet, G.P. Knapik, B. Xie, HTRF: a technology tailored for drug discovery - a review of theoretical aspects and recent applications, Curr. Chem. Genomics 3 (2009) 22–32, https://doi.org/10.2174/1875397300903010022.
[67] B. Heltweg, F. Dequiedt, E. Verdin, M. Jung, Nonisotopic substrate for assaying both human zinc and NAD+-dependent histone deacetylases, Anal. Biochem. 319 (1) (2003) 42–48, https://doi.org/10.1016/S0003-2697(03)00276-8.
[68] T.B. Toro, T.J. Watt, KDAC8 substrate specificity quantified by a biologically relevant, label-free deacetylation assay, Protein Sci. 24 (12) (2015) 2020–2032, https://doi.org/10.1002/pro.2813.
[69] R. Baba, Y. Hori, S. Mizukami, K. Kikuchi, Development of a fluorogenic probe with a transesterification switch for detection of histone deacetylase activity, J. Am. Chem. Soc. 134 (35) (2012) 14310–14313, https://doi.org/10.1021/ja306045j.
[70] R. Baba, Y. Hori, K. Kikuchi, Intramolecular long-distance nucleophilic reactions as a rapid fluorogenic switch applicable to the detection of enzymatic activity, Chemistry 21 (12) (2015) 4695–4702, https://doi.org/10.1002/chem.201406093.
[71] Y. Xie, J. Ge, H. Lei, B.o. Peng, H. Zhang, D. Wang, S. Pan, G. Chen, L. Chen, Y. i. Wang, Q. Hao, S.Q. Yao, H. Sun, Fluorescent probes for single-step detection and proteomic profiling of histone deacetylases, J. Am. Chem. Soc. 138 (48) (2016) 15596–15604, https://doi.org/10.1021/jacs.6b0733410.1021/jacs.6b07334.s001.
[72] C. Wang, W. Du, T. Zhang, G. Liang, A bioluminescent probe for simultaneously imaging esterase and histone deacetylase activity in a tumor, Anal. Chem. 92 (23) (2020) 15275–15279, https://doi.org/10.1021/acs.analchem.0c0422710.1021/acs.analchem.0c04227.s001.
[73] D.R. Rooker, D. Buccella, Real-time detection of histone deacetylase activity with a small molecule fluorescent and spectrophotometric probe, Chem. Sci. 6 (11) (2015) 6456–6461, https://doi.org/10.1039/C5SC02704G.
[74] D.R. Rooker, Y. Klyubka, R. Gautam, E. Tomat, D. Buccella, Peptide-based fluorescent probes for deacetylase and decrotonylase activity: toward a general platform for real-time detection of lysine deacylation, Chembiochem 19 (5) (2018) 496–504, https://doi.org/10.1002/cbic.v19.510.1002/cbic.201700582.
[75] W. Xuan, A. Yao, P.G. Schultz, Genetically encoded fluorescent probe for detecting sirtuins in living cells, J. Am. Chem. Soc. 139 (36) (2017) 12350–12353, https://doi.org/10.1021/jacs.7b0572510.1021/jacs.7b05725.s001.
[76] B.C. Smith, W.C. Hallows, J.M. Denu, A continuous microplate assay for sirtuins and nicotinamide-producing enzymes, Anal. Biochem. 394 (1) (2009) 101–109, https://doi.org/10.1016/j.ab.2009.07.019.
[77] C. Yu, Y. Wu, F. Zeng, X. Li, J. Shi, S. Wu, Hyperbranched polyester-based fluorescent probe for histone deacetylase via aggregation-induced emission, Biomacromolecules 14 (12) (2013) 4507–4514, https://doi.org/10.1021/bm401548u.
[78] K. Dhara, Y. Hori, R. Baba, K. Kikuchi, A fluorescent probe for detection of histone deacetylase activity based on aggregation-induced emission, Chem. Commun. (Camb) 48 (2012) 11534–11536, https://doi.org/10.1039/c2cc36591j.
[79] M. Minoshima, T. Matsumoto, K. Kikuchi, Development of a fluorogenic probe based on a DNA staining dye for continuous monitoring of the histone deacetylase reaction, Anal. Chem. 86 (15) (2014) 7925–7930, https://doi.org/10.1021/ac501881s.
[80] Y. Han, H. Li, Y. Hu, P. Li, H. Wang, Z. Nie, S. Yao, Time-resolved luminescence biosensor for continuous activity detection of protein acetylation-related enzymes based on DNA-sensitized terbium(III) probes, Anal. Chem. 87 (18) (2015) 9179–9185, https://doi.org/10.1021/acs.analchem.5b01338.
[81] J.C. Milne, P.D. Lambert, S. Schenk, D.P. Carney, J.J. Smith, D.J. Gagne, L. Jin, O. Boss, R.B. Perni, C.B. Vu, J.E. Bemis, R. Xie, J.S. Disch, P.Y. Ng, J.J. Nunes, A. V. Lynch, H. Yang, H. Galonek, K. Israelian, W. Choy, A. Iffland, S. Lavu, O. Medvedik, D.A. Sinclair, J.M. Olefsky, M.R. Jirousek, P.J. Elliott, C. H. Westphal, Small molecule activators of SIRT1 as therapeutics for the treatment of type 2 diabetes, Nature 450 (7170) (2007) 712–716, https://doi.org/10.1038/nature06261.
[82] F. Halley, J. Reinshagen, B. Ellinger, M. Wolf, A.L. Niles, N.J. Evans, T. A. Kirkland, J.M. Wagner, M. Jung, P. Gribbon, S. Gul, A bioluminogenic HDAC activity assay: validation and screening, J. Biomol. Screen. 16 (10) (2011) 1227–1235, https://doi.org/10.1177/1087057111416004.
[83] A. Dose, J.O. Jost, A.C. Spieß, P. Henklein, M. Beyermann, D. Schwarzer, Facile synthesis of colorimetric histone deacetylase substrates, Chem. Commun. (Camb) 48 (2012) 9525–9527, https://doi.org/10.1039/c2cc34422j.
[84] B. Suenkel, F. Fischer, C. Steegborn, Inhibition of the human deacylase Sirtuin 5 by the indole GW5074, Bioorg. Med. Chem. Lett. 23 (1) (2013) 143–146, https://doi.org/10.1016/j.bmcl.2012.10.136.
[85] J.E. Bradner, N. West, M.L. Grachan, E.F. Greenberg, S.J. Haggarty, T. Warnow, R. Mazitschek, Chemical phylogenetics of histone deacetylases, Nat. Chem. Biol. 6 (3) (2010) 238–243, https://doi.org/10.1038/nchembio.313.
[86] T. Ciossek, H. Julius, H. Wieland, T. Maier, T. Beckers, A homogeneous cellular histone deacetylase assay suitable for compound profiling and robotic screening, Anal. Biochem. 372 (1) (2008) 72–81, https://doi.org/10.1016/j.ab.2007.07.024.
[87] A. Lahm, C. Paolini, M. Pallaoro, M.C. Nardi, P. Jones, P. Neddermann, S. Sambucini, M.J. Bottomley, P. Lo Surdo, A. Carfi, U. Koch, R. De Francesco, C. Steinkuhler, P. Gallinari, Unraveling the hidden catalytic activity of vertebrate class IIa histone deacetylases, Proc. Natl. Acad. Sci. U. S. A. 104 (2007) 17335–17340.
[88] D. Wegener, F. Wirsching, D. Riester, A. Schwienhorst, A fluorogenic histone deacetylase assay well suited for high-throughput activity screening, Chem. Biol. 10 (1) (2003) 61–68.
[89] D. Wegener, C. Hildmann, D. Riester, A. Schwienhorst, Improved fluorogenic histone deacetylase assay for high-throughput-screening applications, Anal. Biochem. 321 (2003) 202–208.
[90] D. Wegener, C. Hildmann, D. Riester, A. Schober, F.-J. Meyer-Almes, H. E. Deubzer, I. Oehme, O. Witt, S. Lang, M. Jaensch, V. Makarov, C. Lange, B. Busse, A. Schwienhorst, Identification of novel small-molecule histone deacetylase inhibitors by medium-throughput screening using a fluorigenic assay, Biochem. J. 413 (2008) 143–150, https://doi.org/10.1042/BJ20080536.
[91] I. Galleano, M. Schiedel, M. Jung, A.S. Madsen, C.A. Olsen, A. Continuous, Fluorogenic sirtuin 2 deacylase assay: substrate screening and inhibitor evaluation, J. Med. Chem. 59 (2016) 1021–1031, https://doi.org/10.1021/acs.jmedchem.5b01532.
[92] C. Roessler, C. Tüting, M. Meleshin, C. Steegborn, M. Schutkowski, A novel continuous assay for the deacylase sirtuin 5 and other deacetylases, J. Med. Chem. 58 (18) (2015) 7217–7223, https://doi.org/10.1021/acs.jmedchem.5b00293.
[93] T.GM. Schmidt, A. Skerra, The Strep-tag system for one-step purification and high-affinity detection or capturing of proteins, Nat. Protoc. 2 (6) (2007) 1528–1535, https://doi.org/10.1038/nprot.2007.209.
[94] J.-H. Zhang, T.D.Y. Chung, K.R. Oldenburg, A simple statistical parameter for use in evaluation and validation of high throughput screening assays, J. Biomol. Screen. 4 (2) (1999) 67–73, https://doi.org/10.1177/108705719900400206.
[95] J.L. Feldman, K.E. Dittenhafer-Reed, N. Kudo, J.N. Thelen, A. Ito, M. Yoshida, J. M. Denu, Kinetic and structural basis for acyl-group selectivity and NAD(+) dependence in sirtuin-catalyzed deacylation, Biochemistry 54 (19) (2015) 3037–3050, https://doi.org/10.1021/acs.biochem.5b00150.
[96] W. Gai, H.e. Li, H. Jiang, Y. Long, D. Liu, Crystal structures of SIRT3 reveal that the α2-α3 loop and α3-helix affect the interaction with long-chain acyl lysine, FEBS Lett. 590 (17) (2016) 3019–3028, https://doi.org/10.1002/1873-3468.12345.
[97] H.M. Berman, J. Westbrook, Z. Feng, G. Gilliland, T.N. Bhat, H. Weissig, I. N. Shindyalov, P.E. Bourne, The protein data bank, Nucleic Acids Res. 28 (2000) 235–242, https://doi.org/10.1093/nar/28.1.235.
[98] Molecular Operating Environment (MOE), 2019.01; Chemical Computing Group ULC, 1010 Sherbooke St. West, Suite #910, Montreal, QC, Canada, H3A 2R7, 2021.
[99] J. Wang, R.M. Wolf, J.W. Caldwell, P.A. Kollman, D.A. Case, Development and testing of a general amber force field, J. Comput. Chem. 25 (9) (2004) 1157–1174, https://doi.org/10.1002/(ISSN)1096-987X10.1002/jcc.v25:910.1002/jcc.20035.
[100] G. Jones, P. Willett, R.C. Glen, A.R. Leach, R. Taylor, Development and validation of a genetic algorithm for flexible docking, J. Mol. Biol. 267 (1997) 727–748, https://doi.org/10.1006/jmbi.1996.0897.